nature medicine

Supplementary information

https://doi.org/10.1038/s41591-024-03453-1

Bioaccumulation of microplastics in decedent human brains

In the format provided by the authors and unedited

Bioaccumulation of Microplastics in Decedent Human Brains

Alexander J. Nihart[1†], Marcus A. Garcia[1†], Eliane El Hayek[1†], Rui Liu[1], Marian Olewine[1], Josiah D. Kingston[1], Eliseo F. Castillo[2], Rama R. Gullapalli[3], Tamara Howard[4], Barry Bleske[5], Justin Scott[6], Jorge Gonzalez Estrella[6], Jessica M. Gross[7], Michael Spilde[8], Natalie L. Adolphi[9], Daniel F. Gallego[9], Heather S. Jarrell[9], Gabrielle Dvorscak[9], Maria E. Zuluaga-Ruiz[10], Andrew West[11], Matthew J. Campen[1*]

[1] Department of Pharmaceutical Sciences, College of Pharmacy, University of New Mexico Health Sciences, Albuquerque, NM, USA

[2] Division of Gastroenterology and Hepatology, Department of Internal Medicine; [3] Department of Pathology; [4]Department of Cell Biology and Physiology, School of Medicine, University of New Mexico Health Sciences Center, Albuquerque, NM, USA

[5] Department of Pharmacy Practice and Administrative Sciences, College of Pharmacy, University of New Mexico Health Sciences Center, Albuquerque, NM, USA

[6] School of Civil & Environmental Engineering, Oklahoma State University, Stillwater, OK, USA

[7] Clinical and Translational Science Center, University of New Mexico Health Sciences Center, Albuquerque, NM, USA

[8] Department of Earth and Planetary Sciences, University of New Mexico, Albuquerque, NM, USA

[9] Office of the Medical Investigator, University of New Mexico, Albuquerque, NM, USA

[10] Grupo de Investigación en Rehabilitación de la Universidad del Valle - GIRUV, Cali, Colombia

[11] Duke Center for Neurodegeneration and Neurotherapeutics, Duke University, Durham, NC, USA.

† Contributed equally to this manuscript

* Corresponding Author

Matthew J Campen, PhD, Department of Pharmaceutical Sciences, MSC09 5360, 1 University of New Mexico, Albuquerque, NM 87131-0001, (505) 272-5569

Email: MCampen@salud.unm.edu

ORCID ID: 0000-0002-2292-5050

Running Title: Bioaccumulation of microplastics in human brain

Statement of Interests: The authors declare no conflicts of interest with the content of this manuscript.

Table of Contents

1. SUPPLEMENTAL MATERIALS AND METHODS

1.1. Sample Collection at Autopsy.

Samples from the New Mexico Office of the Medical Investigator (NM OMI, “2016 NM OMI,” “2024 NM OMI,” “NM Dementia,” Supplemental Table 1) were collected fresh at the time of autopsy. The bodies were pronounced dead and then transported the same day to the OMI, where they were placed under refrigeration until the following day when a full autopsy with organ dissection was performed. Small pieces of tissue were stored in stock jars with 10% formalin. Kidney and liver tissues were examined immediately at autopsy before fixation in formalin. From the liver, a section was obtained from the right central parenchyma; from the kidney, we obtained a wedge piece of kidney containing cortex (at the base) and medulla (apex). Most brain specimens (frontal cortex) were cut fresh along with the other organs, although some were fixed in formalin for one or two weeks prior to a neuropathology exam. Whole brains were placed in plastic buckets with 20% formalin, then cut and examined. Small pieces of tissue from these brains were also stored in stock jars with 10% formalin.

Formalin was prepared in-house, and all protocols have been consistent from 2013 to the present. Dissection instrumentation was stainless steel, and the cutting boards were made of polyethylene. The only known potential exposure to exogenous plastic was from the cutting boards, plastic stock jars, and plastic brain buckets. Different pathologists at NM OMI obtained samples in 2016 and 2024, but Dr. Gallego conducted all retrievals from the stock jars. Samples were retrieved at random for analysis. Importantly for the present study, the instrumentation and collection environment were identical across organs and for both 2016 and 2024 collections. Cases in the NM OMI include suspected homicides, suicides, accidents, and natural deaths. Additionally, 12 dementia samples (“NM Dementia”, Supplemental Table 1) were supplied through the New Mexico Brain Bank.

Dementia diagnosis was confirmed through the assessment of various histological and immunohistochemical markers. Briefly, formalin -fixed brains were rinsed with water and placed on a cutting board, where the neuropathologist performed a gross external examination, followed by serial sectioning at 0.5 to 1 cm intervals. The examination focused on identifying atherosclerosis, hemorrhages, atrophy, and any visible lesions. Hematoxylin and eosin (H&E)-stained slides were prepared from key regions, including the hippocampus, frontal cortex, basal ganglia, amygdala, thalamus, occipital cortex, midbrain, pons, medulla, and cerebellum. These H&E sections were evaluated for the presence of neuritic and diffuse plaques and neurofibrillary tangles, which were further confirmed using tau immunohistochemical stain. The H&E slide evaluations were used to differentiate various types of dementia, such as Alzheimer, vascular dementia, frontotemporal dementia, Lewy body dementia, and other brain conditions, including demyelination, inflammation, or infection. Immunohistochemical staining for p-tau, beta-amyloid, and TDP-43 were used at the discretion of the neuropathologist.

"East Coast" brain tissue samples (Supplemental Table 1) included fresh-frozen frontal cortex or anterior prefrontal cortex samples from the Duke Kathleen Price Bryan Brain Bank (n=13), and frozen brain samples acquired through the Autism Tissue Program, with samples originating from two different brain banks: the Harvard Brain Tissue Resource Center (n=5) and the NICHD Brain and Tissue Bank at the University of Maryland (n=9). All "East Coast" brain samples were obtained post-mortem and written informed consent was obtained from next-of-kin or legal guardian. "East Coast" samples were from neurologically normal individuals with a variety of causes of death typical for the age group.

Table S1. Summary of available demographic data for brain samples obtained for plastics analysis.

	2016 NM OMI	**2024 NM OMI**	**NM Dementia**	**East Coast**		
				NC	**MD**	**MA**
N	28	24	12	13	9	5
Age (mean, SD)	45.0, 17.3	51.4, 16.0	77.1, 8.7	84	12.9	36.6
Sex (Female/Male/ Undetermined)	10/17/1	10/14/0	5/7/0	6/7/0	1/8/0	1/4/0
Race (White/Native American/African American)	25/2/1	18/5/1	7/1/0[†]	NA		
Ethnicity (Hispanic/ Non-Hispanic)	11/17	7/16	NA	NA		
Collection dates	January-December, 2016	October 2023-January 2024	2019-2024	1997-2013	2000-2005	2004-2005
Cause of Death						
Violence/trauma	9	9	NA	NA		
Substance Use	12	2	NA	NA		
Natural Disease	7	13	NA	NA		
Liver Total Plastics (µg/g)						
Minimum	22.31	63.59	NA	NA		
25% Percentile	54.50	111.4	NA	NA		
Median	**103.7**	**432.9**	NA	NA		
Mean	**141.9**	**465.3**				
75% Percentile	184.9	640.8	NA	NA		
Maximum	412.3	1264	NA	NA		
Kidney Total Plastics (µg/g)						

Minimum	47.80	59.06	NA	NA		
25% Percentile	310.6	213.7	NA	NA		
Median	**402.5**	**404.8**	NA	NA		
Mean	**538.1**	**666.3**				
75% Percentile	786.1	1186	NA	NA		
Maximum	1741	1848	NA	NA		
Brain (Frontal Cortex) Total Plastics (µg/g)						
Minimum	298.5	2216	12806††	74.7	296.3	456.7
25% Percentile	1267	4026	17629††	368.2	687.8	469.6
Median	**3345**	**4917**	**26076††**	**1282**	**1254**	**1013**
Mean	**3420**	**4763**	**27215††**	**1259**	**1404**	**994.8**
75% Percentile	5213	5608	35831††	2085	2348	1511
Maximum	8861	6791	47730††	2627	2685	1744

†n=4 dementia cases had no race identified. ††Py-GC/MS data based on a single KOH digestion and methodologically comparable to other groups, but subsequent benzene removal of lipids reduced values (see below). NA, data not available. NC: Duke Kathleen Price Bryan Brain Bank; MD = NICHD Brain and Tissue Bank at the University of Maryland; MA = Harvard Brain Tissue Resource Center.

The average age of 2016 NM OMI decedents was 45.0 years and the average age of 2024 decedents was 51.4 (Figure S1). A Student's *t*-test revealed no significant difference (p=0.36). Sex, ethnicity, and cause of death varied modestly among groups, but ultimately did not influence MNP concentration outcomes (see details on the multiple regression analysis in section 1.8. below).

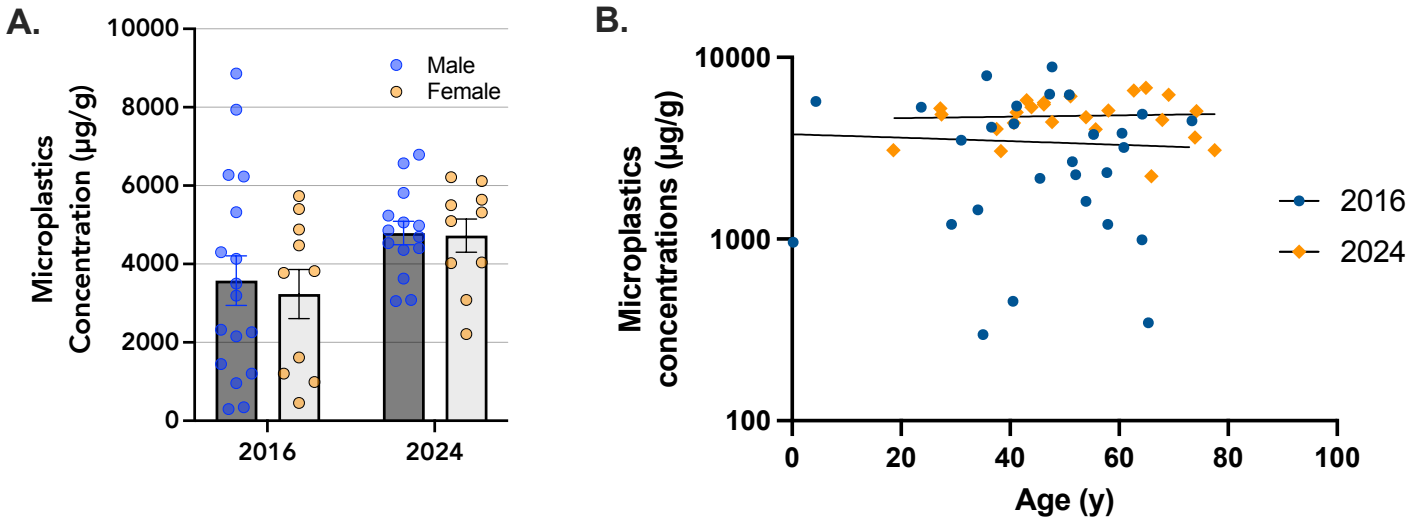

Figure S1. Decedent demographics data relative to MNP concentrations. (A) Microplastics distribution across sex for each collection period (mean ± SD are shown). (B) Lack of association between tissue concentrations and age of subject.

1.2. Pyrolysis Gas Chromatography Mass Spectrometry (PY-GC/MS)

Samples were prepared with intentional avoidance of plastic contamination. Samples from the OMI collection (brain, liver, kidney) were dissected with stainless steel instruments on glass to portions weighing approximately 500 mg and then incubated in 10% potassium hydroxide at 40°C for 3-5 days in glass vials. The resultant digested sample (~1 ml) was transferred into polycarbonate

ultracentrifuge tubes and 200 µl of 100% ethanol was added. Fully digested samples were ultracentrifuged at 100,000 x g for 4h. The resulting pellet was washed 3x with ethanol and dried. A ~1 mg portion of this remaining pellet was run on the Py-GC/MS.

Both UNM and OSU operated an Agilent 8890 GC/5975 MS system (Agilent, Santa Clara, Ca) with an EGA/PY-3030D Pyrolysis Unit (Frontier Labs, Koriyama, Japan) attached to the back inlet. A UAMP column (length 30 m, i.d. 0.25 mm, film thickness: 0.25 µm) and vent free splitter was attached. The pyrolysis settings consisted of temperature set at 600°C and analysis mode was single-shot. The GC/MS settings (Table S2) consisted of inlet temperature (300°C), MS source temperature (250°C), starting oven temperature (40°C), and inlet pressure (10.437 mL/min). The column was initially held at 40°C for 2 mins and ramped up to 280°C at 20°C/min for 10 mins. Then, the temperature increased to 320°C at 40°C/min and maintained there for 15 mins. The experiment was conducted in split injection and the split ratio was 1:50. The twelve polymers of interest are polyethylene (PE), polypropylene (PP), polystyrene (PS), acrylonitrile-butadiene-styrene resin (ABS), sytrene-butadiene rubber (SBR), polymethyl methacrylate (PMMA), polycarbonate (PC), polyvinyl chloride (PVC), polyurethane (PU), polyethylene terephthalate (PET), nylon-6 (N6), and nylon-6,6 (N66). Pyrolyzates for each are shown in Table S3. The calibration curve was created by using MPs-$CaCO_3$ calibration standard at 5 different weights (0.1 mg, 0.2 mg, 0.5 mg, 2 mg, and 4 mg); calibration curves with R^2>0.98 were considered acceptable and rerun if not. Pyrolysis spectra were identified and quantified using F-Search MPs software (version 3.7, Frontier Labs, Koriyama, Japan). F-Search MPs software utilized advanced algorithms to match the obtained spectra with an extensive database, identifying each compound based on its unique spectral fingerprint.

Table S2. Pyrolysis gas chromatography mass spectrometry settings.

Micro furnace pyrolyzer	**EGA/PY-3030D Pyrolysis unit**
Mode	Single shot
Carrier gas	Helium
Temperature	600ºc
Pyrolysis time	0.2 minutes (pyrolysis) 40 minutes total run time for method per sample
Transfer line temperature	280ºc
Gas chromatograph	**Agilent 6890 GC/5975 MS system (Agilent, Santa Clara, CA)**
Injector	50:1
Mode	split
Temperature	300ºc
Column	Ultra Alloy microplastics (UAMP) Column kit specifically designed for microplastics analysis (UA5-30M- 0.5F, Frontier Labs, Koriyama, Japan
Flow (const.) or pressure (cons)	14.3 psi
Temperature program	40ºc hold 2 minutes Ramp @20ºc/min to 280ºc hold for 10 minutes Ramp @40ºc/min to 320ºc hold for 15min
Tranfer line temperature	280ºc
Mass spectrometer	
Ionization energy	69.9 (70eV)
Scan rate	3.42 scan/s
Scan range	30-450

Table S3. Pyrolyzates used for identification and quantification of polymers of interest.

Polymer of Interest	Extracted-Ion Chromatogram Spectrum (EIC) (Main)	Extracted-Ion Chromatogram Spectrum (EIC) (Sub)	**Pyrolyzate Compounds**
Polyethylene (PE)	m/z: 82 1,20-Heneicosadiene (C21")	m/z: 294 1,20-Heneicosadiene (C21")	m/z: 83 1-Dodecene (C12) m/z: 83 1-Hexadecene (C16)
Polypropylene (PP)	m/z: 126 2,4-Dimethyl-1-heptene (C9')	m/z: 70 2,4-Dimethyl-1-heptene (C9')	m/z: 97 2,4,6-Trimethyl-1-nonene m/z: 69 2,4,6,8-Tetramethyl-1-undecene
Polyvinyl Chloride (PVC)	m/z: 128 Naphthalene (Naph)	m/z: 115 Naphthalene (Naph)	m/z: 91 Toluene m/z: 116 Indene m/z: 78 Benzene
Polyethylene Terephthalate (PET)	m/z: 182 Benzophenone (BP)	m/z: 105 Benzophenone (BP)	m/z: 78 Benzene m/z: 122 Benzoic Acid m/z: 154 Diphenyl
Polystyrene (PS)	m/z: 91 Styrene Trimer (SSS)	m/z: 312 Styrene Trimer (SSS)	m/z:104 Styrene m/z:130 Styrene Dimer
Polycarbonate (PC)	m/z: 134 4-isopropenylphenol (IPP)	m/z: 119 4-isopropenylphenol (IPP)	m/z: 94 Phenol
Polyurethane (PU)	m/z: 198 4,4'-Methylenedianiline (MDA)	m/z: 106 4,4'-Methylenedianiline (MDA)	
Styrene Butadiene Rubber (SBR)	m/z: 104 4-Phenylcyclohexene (SB)	m/z: 158 4-Phenylcyclohexene (SB)	m/z: 104 Styrene m/z: 162 Butadiene Trimer ($C_{12}H_{18}$)
Polymethyl Methacrylate (PMMA)	m/z: 100 Methyl Methacrylate (MMA)	m/z: 69 Methyl Methacrylate (MMA)	m/z: 55,85 methyl acrylate
Acronitrile Butadiene Styrene Resin (ABS)	m/z: 170 2-Phenethyl-4-phenylpent-4-enenitrile (SAS)	m/z: 91 2-Phenethyl-4-phenylpent-4-enenitrile (SAS)	m/z: 91 2-Methylene-4-phenylbutanenitrile m/z: 144 2-methylene-4-phenylheptanedinitrile
Nylon 6 (N6)	m/z: 113 ε-Caprolactam (Capro)	m/z: 85 ε-Caprolactam (Capro)	

Nylon 66 (N66)	m/z: 84 Cyclopentanone (CP)	m/z: 55 Cyclopentanone (CP)	m/z:112 1,8-Diazacyclotetradecane-2,7-dione

During mass spectrometry, the pyrolysis products were ionized, and their mass-to-charge ratios (m/z) were measured. F-Search MPs software played a key role in this process, detecting peaks corresponding to ions produced from pyrolysis products. The software then applied algorithms to distinguish real signals from noise, ensuring that only significant peaks were considered for further analysis. The heights of these peaks indicated the ion abundance in experimental samples relative to the calibration standards of known abundance. Example spectra from a brain sample is shown in Figure S2.

In cases where overlapping peaks were present, we performed deconvolution to resolve individual component spectra. This step is crucial for accurately identifying compounds in complex mixtures. The detected peaks were matched against an extensive library of reference spectra within F-Search MPs. Once identified, we utilized the software to quantify the compounds, and validation was performed by comparing them with known standards and cross-referencing them with expected values. This comprehensive evaluation methodology provided high accuracy in identifying and quantifying pyrolysis products, enabling detailed insights into the composition of the samples.

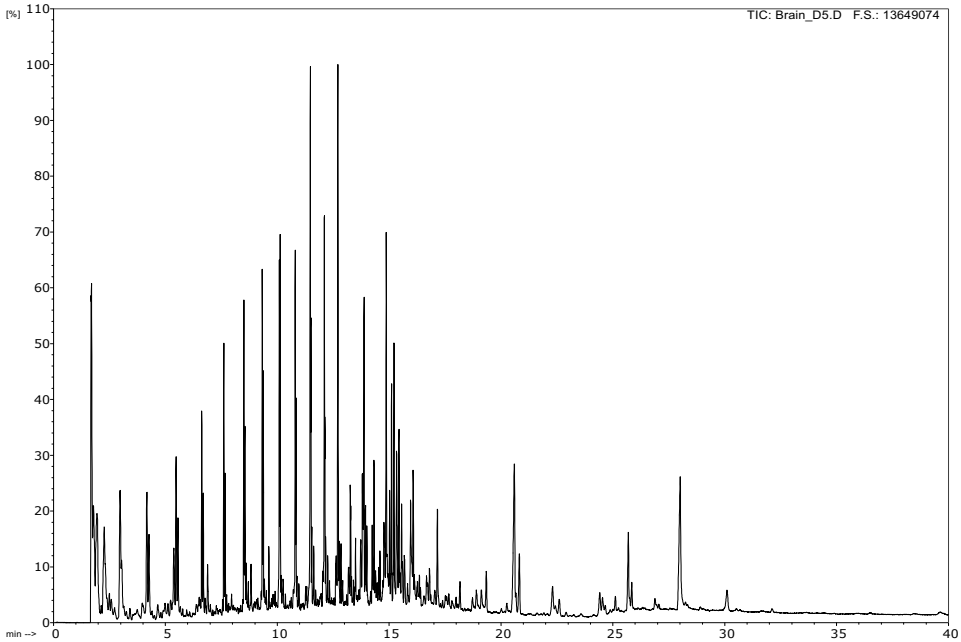

Figure S2. Representative spectra and quantification analysis of isolated MNPs from brain tissue.

For quality control, portions of plastics involved in the process were analyzed separately, including the stock jars and pipette tips (Figure S3). We also analyzed the formalin used in the long-term tissue storage and KOH following ultracentrifugation to confirm the absence of contamination from these sources (Figure S4). Most plastics used in the process are composed of a greater than 4:1 ratio of polypropylene and polyethylene; given that polypropylene was only a small percentage of plastics found in the samples, it is concluded that such fresh plastics used are unlikely to be substantial contributors to the resultant data.

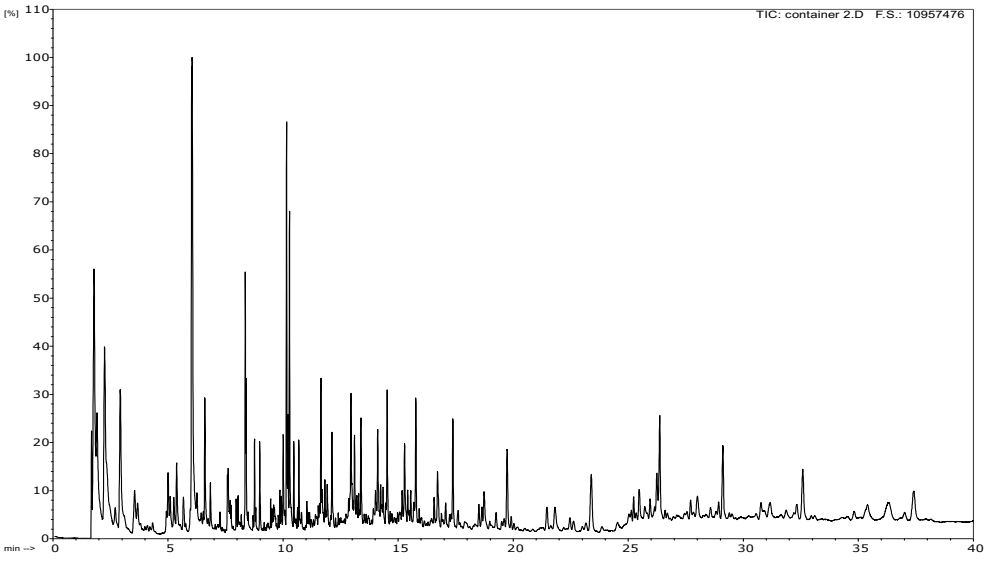

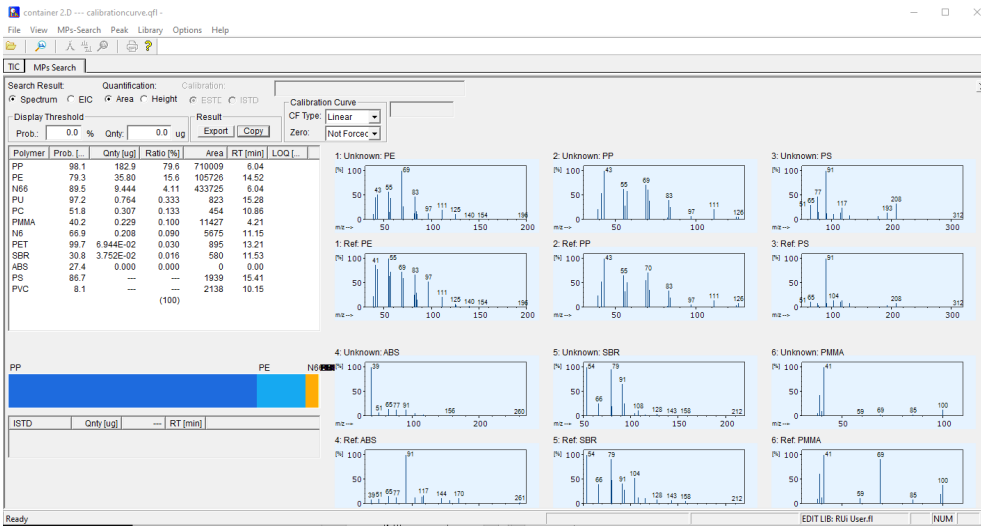

Figure S3. Spectra and quantification analysis of Forensic Evidence collection container used in storing brain tissues. These tubes were a blend of polypropylene (~80%) and polyethylene (16%).

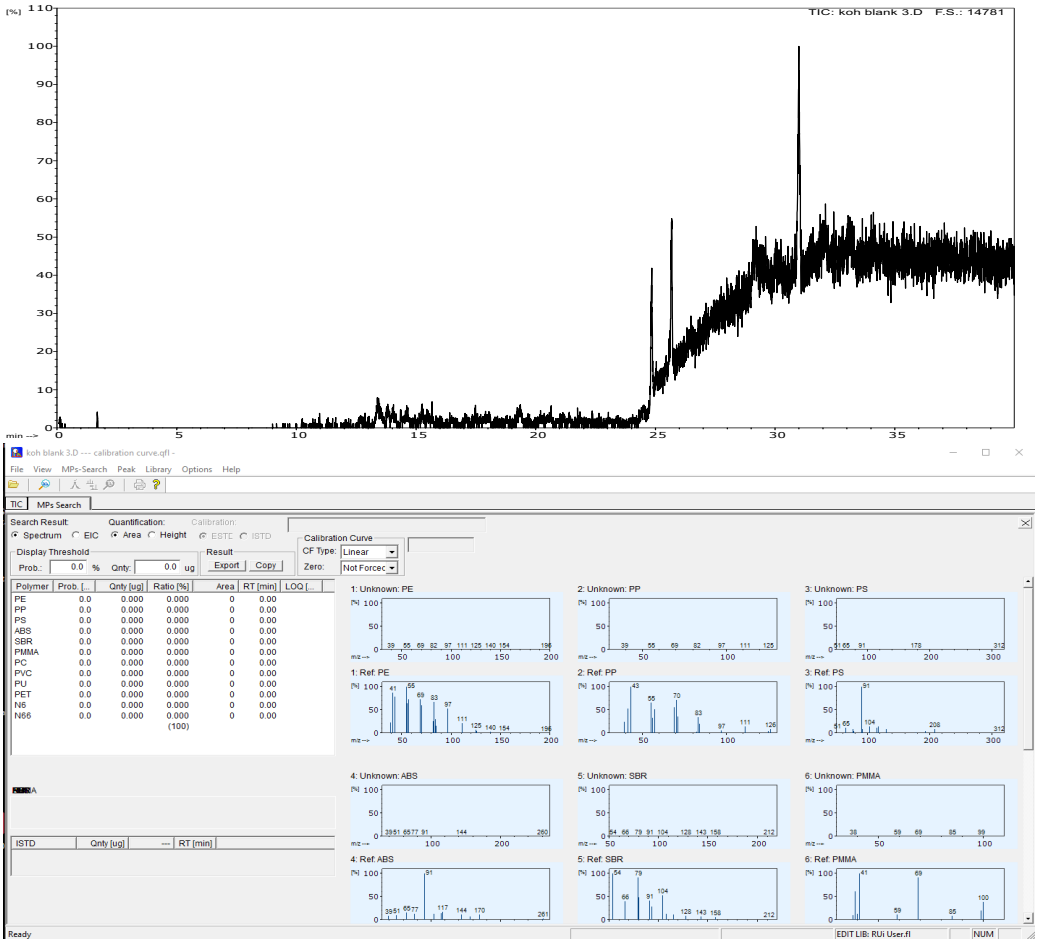

Figure S4. Spectra and quantification of buffers exposed to the experimental pipeline for MNP isolation used in the analysis of all tissues. Here, KOH solution was incubated in HDPE ultracentrifuge tubes for a 4h ultracentrifugation, plus 1h for storage and transport, KOH was added to pyrolysis stainless steel cup and analyzed with no detectable contamination from polymers.

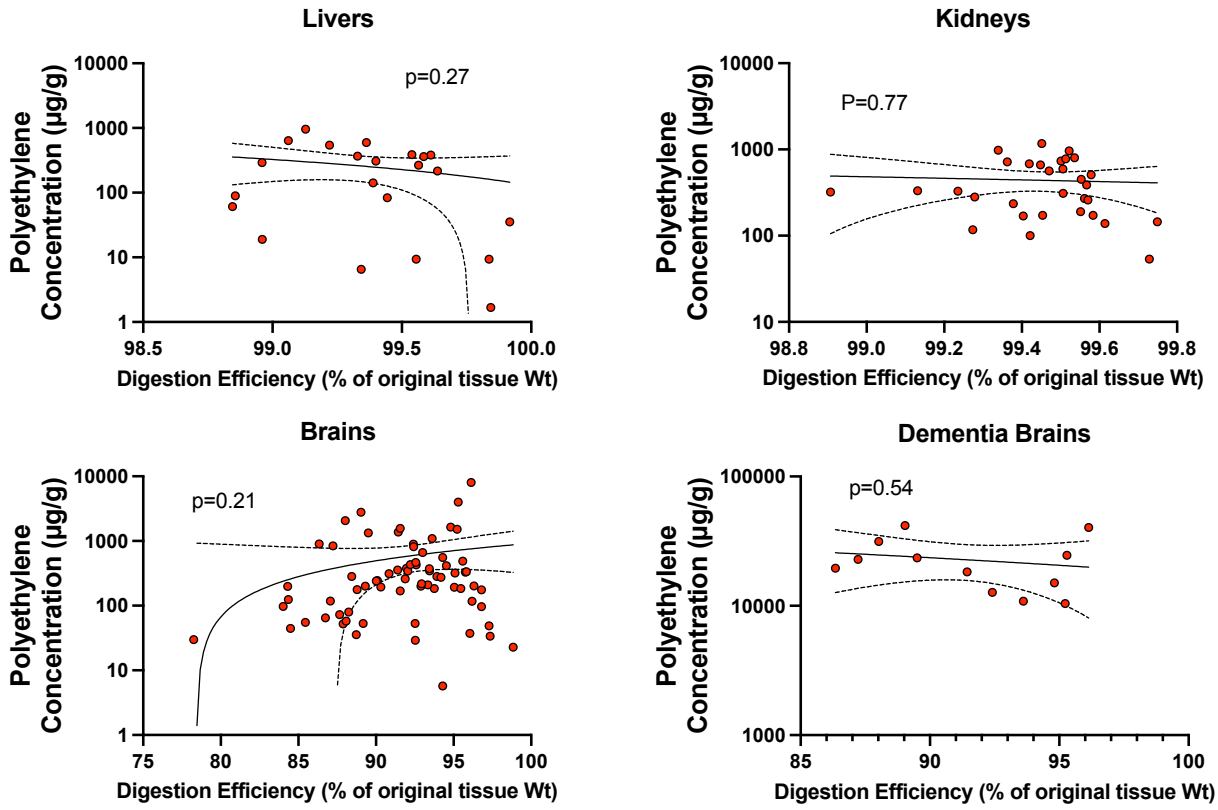

Figure S5. Digestion efficiencies of all liver, kidney, brain and dementia brain samples. Efficiency was calculated as 100 x (1 – postdigestion weight/predigestion weight). No relationship between the efficiency of digestion and polymer content was observed. Linear regression analysis revealed no evidence that trends were significantly non-zero (dashed lines reflect 95% CI; GraphPad Prism).

1.3. Transmission Electron Microscopy (TEM) and Scanning Electron Microscopy Energy-Dispersive Spectroscopy (SEM-EDS)

To assess the size distribution of the extracted particulates from the brain, liver, and kidney, we prepared at least triplicate samples from each organ by suspending the pellet of particulates in 100% ethanol. Particles were deposited on copper TEM mesh grids covered with a holey carbon support film. The grids were not stained and were observed in a Hitachi HT7700 TEM operated at 80 kV. The images were acquired with an AMT XR16M digital camera.

Liver, kidney, and brain sections from decedent samples were analyzed using SEM-EDS parallel with polarization wave microscopy analysis (below). Tissue sections were deparaffinized, washed in 100% and 70% ethanol, and then air-dried overnight in a covered chamber (Petri dish) after being washed in water. The samples were then exposed to osmium vapor for 1h. Finally, to prevent charging, samples were coated with a thin layer of gold and palladium for SEM imaging and EDS analyses. SEM images were made with TESCAN Vega3 using accelerating voltages of 10 to 15 kV and beam currents of 1-4 nA. Secondary electron (SE) and backscattered electron (BSE) imaging, coupled with EDS analyses were used to identify plastic particles. Although SEM-EDS is considered a semi-quantitative analysis, the detected particles in the different tissue sections showed a typically higher carbon count than the tissue and the background of the glass slide.

1.4. Polarization Polarizing Wave Microscopy (PWM)

Refractile body imaging analysis was performed using the polarizing wave microscopy (PWM) technique. A customized PWM microscopy set up was built using an Olympus BX41 microscope (Evident Scientific, Waltham USA). PWM imaging set up includes the following components in order – 1. broadband, unpolarized light source (400-700 nm); 2. optical polarizer; 3. tissue sample; 4. full wavelength (λ) retardance plate; 5. polarization analyzer; and 6. imaging camera. Decedent tissue slides (liver, kidney and brain) were stained with Hematoxylin and Eosin (H & E) first. All H & E slides were examined sequentially using Olympus UPlanSApo objectives (10X, 20X, 40X and 60X) using brightfield imaging first followed by PWM examination. Particle birefringence was confirmed using a full-wavelength (λ) retarder first prior to detailed examination. Refractile bodies in the tissue plane at the center of the specimen alone were considered for imaging analysis to reduce false positives.

1.5. Sample Preparation for Spectroscopy

Samples consisted of five representative homogenized and previously digested brain tissue (2016) pellets labeled B1-B2-B3-B4-B5. Pellets were distributed using a stainless-steel micro spatula and weighed using a precision balance (Mettler Toledo XP2U, USA). Pellets were then separated into aliquots for particle imaging and Nile Red particle quantification followed by analysis using Reflectance and Attenuated Total Reflectance-Fourier-transform infrared spectroscopy (ATR-FTIR) and pyrolysis gas chromatography mass spectrum (Py-GC/MS). Glass vessels were used for the remaining experiments to avoid plastic contamination. Sample aliquots for imaging and Nile Red particle quantification, and ATR-FTIR were suspended into 10 mL of ultra-pure water and vortexed to bring to solution and sonicated for 10 min. To remove salt particle interferences, the solution was adjusted to a pH of 2.5 by adding 50 µL of nitric acid, followed by vortexing and sonicating for another 10 min. The extracted particles were carefully transferred to a 25 mm-diameter, 0.2 µm aluminum oxide (Al_2O_3) filter under the fume hood using a glass pipette. For Py-GC/MS, aliquots were weighed out into stainless steel furnace cups for analysis.

1.6. Imaging and Nile Red Particle Quantification

Each of the five sample's Al_2O_3 filters and a control blank (consisting of ultra-pure water prepared identical to the samples) were stained with 60 µL of a 30 µg of Nile Red per mL methanol solution for particle quantification. The filters were left to react with the dye for 10 min, then were rinsed with 600 µL of n-hexane on a glass filtration stack to remove excess dye. Each filter was imaged with a stereomicroscope (AmScope 7X-180X Trinocular Zoom Stereo Microscope) for initial visual identification. The six filters were placed on a Greiner 6-well plate and imaged using a fluorescence microscope (Cytation 5 Cell Imaging Multi-Mode Reader, Agilent Technologies). A series of images were taken at 4X magnification with an RFP filter cube (excitation 531 nm/emission 593 nm) to produce a stitched image of each filter using Gen5® software. The detection limit of Cytation 5 cell Imaging at this magnification is ~ 0.5 µm. Each image was preprocessed to reduce background fluorescence. Further reduction of background fluorescence was made by increasing image contrast and decreasing brightness. Each preprocessed image was run through the MPVAT 2.0[1] macros three times using ImageJ and the average with standard deviations was reported. Only the filter flow-through area was considered for quantification.

1.7. Microplastic Analysis by Attenuated Total Reflectance-Fourier-transform Infrared Spectroscopy with (ATR-FTIR)

Each filter was mounted on a gold mirror slide for particle identification with a FTIR spectrometer (Thermo Nicolet iN10 MX). First, using the reflectance detector, a mosaic image of the filter flow-through area was taken using OMNIC Picta® software and a heat map was established with spectra being quantified for particle identification. Each measurement was taken using a 90 sec detection time with 256 scans, a spectral range of 4000-675 cm^{-1}, number of points consisted of 10 X and 13 Y, with a step size of 100 µm by 100 µm, aperture width of 150 µm and height of 150 µm, and a spectral resolution of 4 cm^{-1}. Another mosaic map was acquired to guide the selection of potential plastic particles for further examination using a cooled ATR detector and germanium tip. The aperture size of the ATR detector was adapted to fit each particle. The number of particles examined with ATR-FTIR was about 10% of the particles identified during fluorescence microscopy quantification, or at least ten points, whichever was greater. The number of particles for the control blank consisted of only one point due to a lack of particles present. Each measurement was taken using a 90 sec detection time with 256 scans, a spectral range of 4000-675 cm^{-1}, with an aperture width of 150 µm and height of 150 µm and a spectral resolution of 4 cm^{-1}. The resulting spectra were searched against the HR Polymer Additives and Plasticizers, Hummel Polymer Sample Library, Polymer Laminate Films, and Synthetic Fibers by Microscope libraries. A good match (%) with the polymer type is considered a value greater than 60%. Backgrounds were collected before each sample point and mosaic heat mapping.

1.8. Statistical Analysis

Normality Assessment of 2016 and 2024 Decedent Data. Data for each organ at the two separate dates of death were analyzed for normality (Table S4) and lognormality (Table S5) using the Shapiro-Wilk test (GraphPad Prism v10.4.0). Kidney and liver samples were both lognormally distributed. Brains samples had more consistently normal distributions.

Table S4. Normality test for untransformed total plastics concentrations

Shapiro-Wilk test	Liver ‘16	Liver ‘24	Kidney ‘16	Kidney ‘24	Brain ‘16	Brain ‘24
W	0.8969	0.9114	0.8775	0.8698	0.9434	0.9669
P value	0.0114	0.0436	0.0108	0.0116	0.0854	0.6393
Passed **normality** test (alpha=0.05)?	No	No	No	No	Yes	Yes
P value summary	*	*	*	*	ns	ns

Table S5. Lognormality test for untransformed total plastics concentrations

Shapiro-Wilk test	Liver ‘16	Liver ‘24	Kidney ‘16	Kidney ‘24	Brain ‘16	Brain ‘24
W	0.9693	0.9143	0.9556	0.9395	0.9305	0.9180
P value	0.5826	0.0504	0.4064	0.2348	0.0363	0.0691
Passed **lognormality** test (alpha=0.05)?	Yes	Yes	Yes	Yes	No	Yes
P value summary	ns	ns	ns	ns	*	ns

Data were log-transformed and the normality test was rerun. Log-transformed data were all normally distributed (Table S6). The two-way Analysis of Variance (ANOVA) was run on a log-transformed data (below) as this most fully met the standards for normal distribution among all samples.

Table S6. Normality test for log-transformed total plastics concentrations

Shapiro-Wilk test of Log-Transformed Data	Liver '16	Liver '24	Kidney '16	Kidney '24	Brain '16	Brain '24
W	0.9693	0.9143	0.9556	0.9395	0.9407	0.9180
P value	0.5826	0.0504	0.4064	0.2348	0.0647	0.0691
Passed **normality** test (alpha=0.05)?	Yes	Yes	Yes	Yes	Yes	Yes
P value summary	ns	ns	ns	ns	ns	ns

Two-Way Analysis of Variance Considering Organ and Date of Death. For the main manuscript, it was important to convey the real units of concentration in µg/g (see Figure 1A). However, a two-way ANOVA (GraphPad Prism v10.4.0) of the log-transformed data (Table S7) also revealed higher levels of plastics in the brain than in livers or kidneys with an increasing trend over time (Figure S6).

Table S7	All Organ log transform 2-way				
Two-way ANOVA	Ordinary				
Alpha	0.05				
Source of Variation	% of total variation	P value	P value summary	Significant?	
Interaction	1.933	0.0118	*	Yes	
Organ	65.29	<0.0001	****	Yes	
Time	3.015	0.0002	***	Yes	
ANOVA table	**SS (Type III)**	**DF**	**MS**	**F (DFn, DFd)**	**P value**
Interaction	**1.244**	**2**	**0.6220**	**F (2, 136) = 4.591**	**P=0.0118**
Organ	**42.01**	**2**	**21.00**	**F (2, 136) = 155.0**	**P<0.0001**
Time	**1.940**	**1**	**1.940**	**F (1, 136) = 14.32**	**P=0.0002**
Residual	**18.42**	**136**	**0.1355**		
Difference between column means					
Predicted (LS) mean of 2016	2.704				
Predicted (LS) mean of 2024	2.939				
Difference between predicted means	-0.2354				
SE of difference	0.06221				
95% CI of difference	-0.3585 to -0.1124				
Data summary					
Number of columns (Time)	2				
Number of rows (Organ)	3				
Number of values	142				

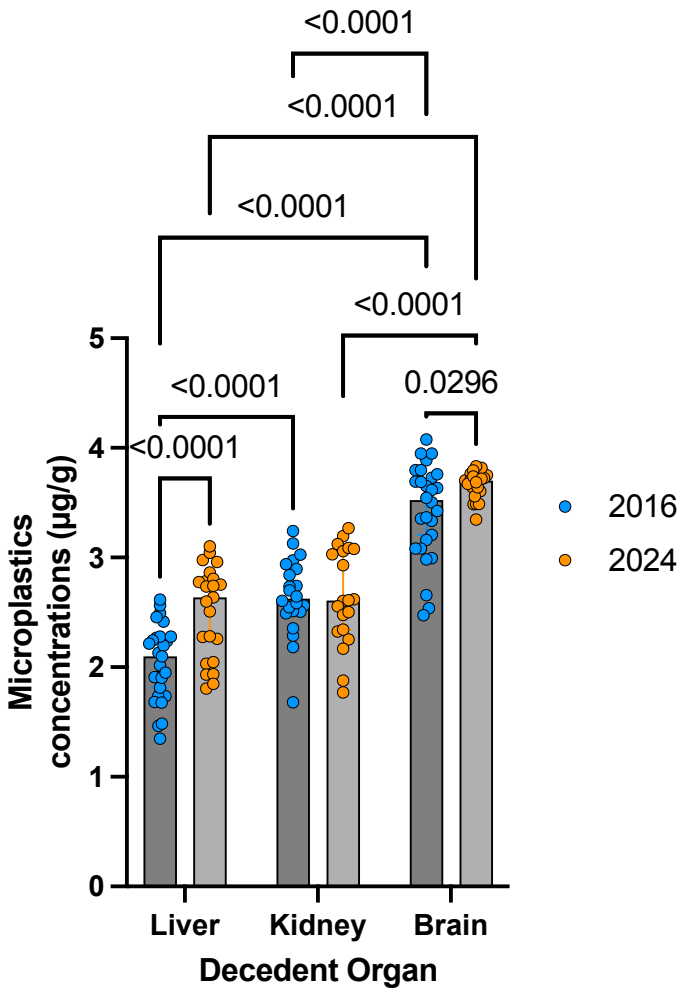

Figure S6. Log-transformed total microplastics concentration, indicating statistical conclusions following a two-way ANOVA with a post-hoc comparison using the original false discovery rate correction method of Benjamini and Hochberg (bars represent median and 95% confidence interval).

Multiple Regression Modeling for Brain Microplastics Content. Limited sample data were available for decedent samples: date of death, sex, age, race/ethnicity, and cause of death (classified as traumatic, substance use-related, or disease). Data preparation for the multiple linear regression included data cleaning. We standardized the sex variable entries “f” and “F” to “female” and “m” and “M” to “male”. One individual was listed as “z” for sex. We conducted the analyses in two ways: first by treating this individual as belonging to a third sex category (separate from male and female), and second, coding this person as having missing data for sex. These two approaches yielded consistent results in terms of model fit, described below, so we present the results only from models where this individual’s sex was coded as missing. Additionally, for the variable race, we combined “Black and “African American” into a single category (“Black/African American”), “AI and “American Indian” into a single category (“Native American”), and “Caucasian” and “White” into a single category ("White”). Ethnicity was already dichotomized into Hispanic and non-Hispanic.

We used multiple linear regression to model the relationship between six independent variables (age, sex, race, ethnicity, cause of death, and date of death) and two dependent variables, LogTotal (log of

the total plastics concentration) and LogPE (log of the polyethylene-only concentrations), conducting a separate analysis for each dependent variable using R version 4.3.3.[2] We tested the assumptions of linear regression including multicollinearity among the independent variables, as well as homoscedasticity and normality of residuals.

These tests showed that the assumption of homoscedasticity was violated for both dependent variables. We therefore also conducted robust multiple linear regression using Huber's M-estimation for both log-transformed and non-transformed outcomes.[3] To identify the best-fit model for each dependent variable, we used a backward elimination approach to stepwise regression and assessed the relative fit of nested models using AIC. We report the full (all independent variables included) and best-fit multiple and robust multiple linear regression models for the log-transformed and non-transformed data. We used both p-values and the coefficients with their corresponding confidence intervals to determine significance.

Regression Analysis Outcomes

Brain:

In the full multiple linear regression models, none of the independent variables were significantly associated with either measure of polymer concentration in decedent brains (Table S8). Additionally, neither model's F-statistic was significant, indicating that the model was no better at predicting the dependent variable than chance alone (LogTotal: $F(8, 41)=1.355$, $p=0.24$, and LogPE:$F(8, 41)=1.499$,$p=0.19$). This lack of significance among independent variables may be due to the small sample size (n = 52) paired with the relatively large number of independent variables included in the models (n = 6). The backward elimination process revealed that the best-fit model included only one independent variable: date of death (Table S8). Specifically, death in 2024 was associated with a 0.24 unit increase in LogTotal relative to death in 2016 ($p=0.02$). Similarly, LogPE concentrations were 0.24 units higher in decedents who died in 2024 relative to those who died in 2016 ($p=0.01$).

Given the heteroscedasticity of residuals in the multiple linear regression models, we also conducted robust linear regressions using the log-transformed and non-transformed dependent variables. This method is comparatively robust to the violations of the assumptions of linear regression listed above. The results from the robust linear models were the same in terms of significance for date of death regardless of whether the dependent variable was log-transformed or not; across all full models (prior to backwards elimination), none of the six independent variables were significantly associated with the dependent variables, and the best-fit models consistently included only the date of death.

Multiple linear regression for LogTotal Plastics (full model)

Coefficient	Estimate	SE	t	95% CI		p
				LL	UL	
Intercept	3.46	0.18	19.04	3.09	3.82	0.00
Age	0.00	0.00	-0.07	-0.01	0.01	0.95
Sex: Male	-0.02	0.11	-0.16	-0.24	0.20	0.88
Race: Black/African American	0.30	0.26	1.15	-0.23	0.83	0.26

Race: Native American	0.19	0.15	1.27	-0.11	0.50	0.21
Ethnicity: Non-Hispanic	-0.02	0.12	-0.16	-0.26	0.22	0.87
Cause of Death: Overdose	-0.12	0.13	-0.92	-0.39	0.15	0.37
Cause of Death: Disease	0.08	0.13	0.63	-0.17	0.33	0.53
Date of Death: 2024	0.17	0.11	1.50	-0.06	0.39	0.14
R^2=0.21; Adjusted R^2=0.05; p=0.24						

Best-fit multiple linear regression for LogTotal

Coefficient	Estimate	SE	t	95% CI		p
				LL	UL	
Intercept	3.43	0.06	53.47	3.30	3.55	0.00
Date of Death: 2024	0.24	0.09	2.52	0.05	0.43	0.02
R^2=0.12; Adjusted R^2=0.10; p=0.02						
p<0.05						

Multiple linear regression for LogPE (full model)

Coefficient	Estimate	SE	t	95% CI		p
				LL	UL	
Intercept	3.37	0.17	19.92	3.03	3.71	0.00
Age	0.00	0.00	-0.28	-0.01	0.01	0.78
Sex: Male	-0.04	0.10	-0.38	-0.24	0.17	0.71
Race: Black/African American	0.28	0.24	1.13	-0.22	0.77	0.27
Race: Native American	0.15	0.14	1.03	-0.14	0.43	0.31
Ethnicity: Non-Hispanic	0.01	0.11	0.08	-0.22	0.23	0.94
Cause of Death: Overdose	-0.14	0.12	-1.18	-0.39	0.10	0.25
Cause of Death: Disease	0.06	0.12	0.51	-0.18	0.29	0.61
Date of Death: 2024	0.17	0.10	1.63	-0.04	0.38	0.11
R^2=0.23; Adjusted R^2=0.08; p=0.19						

Best-fit multiple linear regression model for LogPE

Coefficient	Estimate	SE	t	95% CI		p
				LL	UL	
Intercept	3.29	0.06	54.98	3.17	3.42	0.00
Date of Death: 2024	0.24	0.09	2.68	0.06	0.41	0.01
R^2=0.13; Adjusted R^2=0.11; p=0.01						
p<0.05						

Robust multiple regression model for LogTotal Plastics (full model)

Coefficient	Estimate	SE	t	95% CI		p
				LL	UL	
Intercept	3.53	0.16	21.51	3.21	3.86	0.00
Age	0.00	0.00	-0.26	-0.01	0.00	0.80
Sex: Male	-0.02	0.10	-0.16	-0.21	0.18	0.88
Race: Black/African American	0.26	0.24	1.08	-0.21	0.72	0.29
Race: Native American	0.16	0.14	1.20	-0.10	0.43	0.24
Ethnicity: Non-Hispanic	-0.04	0.11	-0.35	-0.25	0.17	0.73
Cause of Death: Overdose	-0.10	0.12	-0.81	-0.33	0.14	0.42
Cause of Death: Disease	0.08	0.11	0.71	-0.14	0.30	0.48
Date of Death: 2024	0.14	0.10	1.34	-0.06	0.33	0.19

Pseudo R-squared = 0.220
Adjusted pseudo R-squared = 0.068

Robust multiple regression model for LogTotal Plastics (best-fit model)

Coefficient	Estimate	SE	t	95% CI		p
				LL	UL	
Intercept	3.49	0.06	62.99	3.38	3.60	0.00
Date of Death: 2024	0.17	0.08	2.09	0.01	0.33	0.04

Pseudo R-squared = 0.126; Adjusted pseudo R-squared = 0.107
p<0.05

Robust multiple regression model for LogPE (full model)

Coefficient	Estimate	SE	t	95% CI		p
				LL	UL	
Intercept	3.41	0.14	23.56	3.12	3.69	0.00
Age	0.00	0.00	-0.28	-0.01	0.00	0.78
Sex: Male	-0.02	0.09	-0.24	-0.19	0.15	0.81
Race: Black/African American	0.26	0.21	1.27	-0.14	0.67	0.21
Race: Native American	0.11	0.12	0.93	-0.12	0.35	0.36
Ethnicity: Non-Hispanic	-0.02	0.10	-0.22	-0.21	0.17	0.82
Cause of Death: Overdose	-0.18	0.10	-1.73	-0.39	0.02	0.09
Cause of Death: Disease	0.06	0.10	0.59	-0.14	0.25	0.56
Date of Death: 2024	0.15	0.09	1.67	-0.03	0.32	0.10

Pseudo R-squared = 0.238
Adjusted pseudo R-squared = 0.090

Robust multiple regression model for LogPE (best-fit model)

Coefficient	Estimate	SE	t	95% CI		p
				LL	UL	
Intercept	3.34	0.05	63.93	3.23	3.44	0.00
Date of Death: 2024	0.19	0.08	2.53	0.04	0.35	0.01

Pseudo R-squared = 0.144

Adjusted pseudo R-squared = 0.090

p<0.05

Robust multiple regression model for Total Plastics (full model)

Coefficient	Estimate	SE	t	95% CI		p
				LL	UL	
Intercept	3644.80	1260.78	2.89	1173.71	6115.89	0.01
Age	-3.90	21.95	-0.18	-46.91	39.11	0.86
Sex: Male	-216.92	756.97	-0.29	-1700.55	1266.71	0.78
Race: Black/African American	2783.42	1817.16	1.53	-778.15	6344.99	0.13
Race: Native American	1552.67	1055.03	1.47	-515.16	3620.49	0.15
Ethnicity: Non-Hispanic	-304.39	832.09	-0.37	-1935.25	1326.47	0.72
Cause of Death: Overdose	-267.39	912.10	-0.29	-2055.08	1520.29	0.77
Cause of Death: Disease	656.73	868.17	0.76	-1044.86	2358.31	0.45
Date of Death: 2024	997.69	775.64	1.29	-522.54	2517.93	0.21

Pseudo R-squared = 0.071

Adjusted pseudo R-squared = -0.110

Robust multiple regression for Total Plastics (best-fit model)

Coefficient	Estimate	SE	t	95% CI		p
				LL	UL	
Intercept	3496.81	400.82	8.72	2711.21	4282.41	0.00
Date of Death: 2024	1283.53	590.98	2.17	125.22	2441.83	0.03

Pseudo R-squared = 0.019

Adjusted pseudo R-squared = -0.002

p<0.05

Robust multiple regression for PE (Full model)

Coefficient	Estimate	SE	t	95% CI		p
				LL	UL	
Intercept	2645.20	854.70	3.09	970.02	4320.37	0.00
Age	-1.64	14.88	-0.11	-30.80	27.52	0.91
Sex: Male	-243.74	513.16	-0.47	-1249.51	762.03	0.64
Race: Black/African American	1963.73	1231.87	1.59	-450.69	4378.16	0.12
Race: Native American	760.82	715.22	1.06	-640.98	2162.62	0.29
Ethnicity: Non-Hispanic	-73.10	564.08	-0.13	-1178.68	1032.48	0.90
Cause of Death: Overdose	-371.18	618.32	-0.60	-1583.07	840.71	0.55
Cause of Death: Disease	291.72	588.54	0.50	-861.80	1445.24	0.62
Date of Death: 2024	846.42	525.82	1.61	-184.16	1877.01	0.12

Pseudo R-squared = 0.062

Adjusted pseudo R-squared = -0.121

Robust multiple regression for PE (best-fit model)						
Coefficient	Estimate	SE	t	95% CI		p
				LL	UL	
Intercept	2486.21	289.47	8.59	1918.85	3053.57	0.00
Date of Death: 2024	1018.84	426.81	2.39	182.32	1855.37	0.02
Pseudo R-squared= 0.028						
Adjusted pseudo R-squared = 0.007						
p<0.05						

Table S8. Collected multiple regression analysis for total plastics and polyethylene in decedent brain specimens from 2016 and 2024, with respect to independent variables date of death, age, sex, race, ethnicity, and cause of death. Both log-transformed and untransformed data were analyzed for rigor.

Kidney:

None of the independent variables were significant at the 0.05 level in the full multiple regression models for either variable, and adjusted R^2 values were low, indicating limited explanatory power (Table S9). Similarly to the brain analyses, the full models' F-statistics were not significant (LogTotal: $F(8, 29) = 1.269$, $p = 0.30$; LogPE: $F(8, 29) = 1.420$, $p = 0.23$).

In each of the best-fit models, we found a significant negative association between ethnicity and the dependent variable (LogTotal ($p = 0.04$) and LogPE ($p = 0.04$)). Since Hispanic was the reference category, this finding indicates that non-Hispanic individuals had lower microplastic concentrations in their kidneys. Age and sex had positive but non-significant effects on both dependent variables.

All assumptions of linear regression were met for LogTotal and LogPE, so robust regression was unnecessary for these variables, and there was no need to analyze the non-transformed data.

Multiple linear regression for LogTotal (full model)						
Coefficient	Estimate	SE	t	95% CI		p
				LL	UL	
Intercept	2.73	0.22	12.41	2.28	3.18	0.00
Age	0.00	0.00	1.10	0.00	0.01	0.28
Sex: Male	-0.19	0.14	-1.34	-0.48	0.10	0.19
Race: Black/African American	0.54	0.41	1.30	-0.31	1.39	0.21
Race: Native American	0.00	0.18	0.03	-0.36	0.37	0.98
Ethnicity: Non-Hispanic	-0.30	0.16	-1.81	-0.63	0.04	0.08
Cause of Death: Overdose	0.11	0.19	0.58	-0.28	0.51	0.57
Cause of Death: Disease	0.01	0.17	0.07	-0.34	0.36	0.95
Date of Death: 2024	0.02	0.15	0.13	-0.29	0.33	0.90
R^2=0.26; Adjusted R^2=0.05; p=0.30						

Best-fit multiple linear regression for LogTotal						
Coefficient	Estimate	SE	t	95% CI		p
				LL	UL	
Intercept	2.76	0.18	15.42	2.40	3.13	0.00

Age	0.01	0.00	1.54	0.00	0.01	0.13
Sex: Male	-0.18	0.13	-1.42	-0.45	0.08	0.16
Ethnicity: Non-Hispanic	-0.29	0.14	-2.09	-0.57	-0.01	0.04

R^2=0.183; Adjusted R^2=0.111;
p=0.073

p<0.05

Multiple linear regression for LogPE (full model)

Coefficient	Estimate	SE	t	95% CI		p
				LL	UL	
Intercept	2.41	0.25	9.46	1.89	2.93	0.00
Age	0.00	0.00	0.73	-0.01	0.01	0.47
Sex: Male	-0.19	0.16	-1.18	-0.53	0.14	0.25
Race: Black/African American	0.50	0.48	1.04	-0.48	1.48	0.31
Race: Native American	-0.09	0.21	-0.44	-0.51	0.33	0.66
Ethnicity: Non-Hispanic	-0.29	0.19	-1.51	-0.67	0.10	0.14
Cause of Death: Overdose	0.25	0.22	1.12	-0.21	0.71	0.27
Cause of Death: Disease	0.13	0.20	0.67	-0.27	0.53	0.51
Date of Death: 2024	0.09	0.18	0.52	-0.27	0.45	0.61

R^2=0.281; Adjusted R^2=0.083; p=0.230

Best-fit multiple linear regression model for LogPE

Coefficient	Estimate	SE	t	95% CI		p
				LL	UL	
Intercept	2.52	0.21	12.09	2.10	2.95	0.00
Age	0.01	0.00	1.60	0.00	0.01	0.12
Sex: Male	-0.23	0.15	-1.54	-0.54	0.07	0.13
Ethnicity: Non-Hispanic	-0.34	0.16	-2.12	-0.67	-0.01	0.04

R^2=0.195; Adjusted R^2=0.124; p=0.06

p<0.05

Table S9. Multiple regression analysis for log-transformed total plastics and polyethylene in decedent kidney specimens from 2016 and 2024, with respect to independent variables date of death, age, sex, race, ethnicity, and cause of death.

Liver:

For LogPE, none of the independent variables were significantly associated in either the full or best-fit model, and the adjusted R^2 values were low (Table S10). The F-statistics were not significant in the full model ($F(8, 38) = 1.02$, $p = 0.438$) or in the best-fit model ($F(3, 43) = 2.32$, $p = 0.089$). However, date of death was significantly and positively associated with LogTotal in both the full ($p < 0.001$) and best-fit models ($p < 0.001$), meaning that the concentration of microplastics was higher in the 2024 sample. The F-statistics were also significant for both the LogTotal full ($F(8, 38) = 3.10$, $p = 0.009$) and the best-fit models ($F(1, 45) = 19.69$, $p < 0.001$).

Again, all assumptions of linear regression were met for LogTotal and LogPE, making robust regression and analysis of the non-transformed data unnecessary.

Multiple linear regression for LogTotal (full model)

Coefficient	Estimate	SE	t	95% CI		p
				LL	UL	
Intercept	1.92	0.18	10.38	1.54	2.29	0.00
Age	0.00	0.00	0.36	-0.01	0.01	0.72
Sex: Male	0.13	0.12	1.14	-0.10	0.37	0.26
Race: Black/African American	0.51	0.39	1.29	-0.29	1.30	0.21
Race: Native American	-0.13	0.15	-0.84	-0.44	0.18	0.41
Ethnicity: Non-Hispanic	-0.05	0.13	-0.39	-0.33	0.22	0.70
Cause of Death: Overdose	0.01	0.16	0.03	-0.32	0.33	0.97
Cause of Death: Disease	0.11	0.14	0.79	-0.18	0.40	0.44
Date of Death: 2024	0.47	0.12	3.89	0.23	0.72	0.00

R^2=0.395; Adjusted R^2=0.268; p=0.009

Best-fit multiple linear regression for LogTotal

Coefficient	Estimate	SE	t	95% CI		p
				LL	UL	
Intercept	2.05	0.07	28.89	1.91	2.20	0.00
Date of Death: 2024	0.47	0.11	4.44	0.26	0.69	0.00

R^2=0.304; Adjusted R^2=0.289; p=0.00005829

$p<0.05$

Multiple linear regression for LogPE (full model)

Coefficient	Estimate	SE	t	95% CI		p
				LL	UL	
Intercept	1.49	0.30	4.96	0.88	2.10	0.00
Age	0.00	0.01	0.88	-0.01	0.01	0.39
Sex: Male	0.16	0.19	0.85	-0.22	0.54	0.40
Race: Black/African American	0.47	0.64	0.74	-0.83	1.77	0.47
Race: Native American	-0.38	0.25	-1.50	-0.89	0.13	0.14
Ethnicity: Non-Hispanic	0.00	0.22	0.01	-0.44	0.45	1.00
Cause of Death: Overdose	0.03	0.26	0.12	-0.49	0.56	0.90
Cause of Death: Disease	0.16	0.23	0.67	-0.31	0.63	0.51
Date of Death: 2024	0.17	0.20	0.85	-0.23	0.57	0.40

R^2=0.177; Adjusted R^2=0.003; p=0.4382

Best-fit multiple linear regression model for LogPE

Coefficient	Estimate	SE	t	95% CI		p
				LL	UL	
Intercept	1.64	0.22	7.35	1.19	2.09	0.00

Age	0.01	0.00	1.63	0.00	0.02	0.11
Race: Black/African American	0.40	0.58	0.68	-0.78	1.57	0.50
Race: Native American	-0.42	0.21	-1.95	-0.85	0.01	0.06

R^2=0.139; Adjusted R^2=0.079; p=0.089

p<0.05

Table S10. Collected multiple regression analysis for log-transformed total plastics and polyethylene in decedent liver specimens from 2016 and 2024, with respect to independent variables date of death, age, sex, race, ethnicity, and cause of death.

2. SUPPLEMENTAL RESULTS

2.1. Additional Imaging

Additional images provided essential perspectives on the nature of particles seen after KOH digestion or in histological sections. Size and shape of particles, along with the anatomical locations of accumulation are highlighted in Figures S7-S14. XDS results of SEM imaging are provided in Extended Data Figures 4-7 to highlight the carbon-rich nature of these particulates.

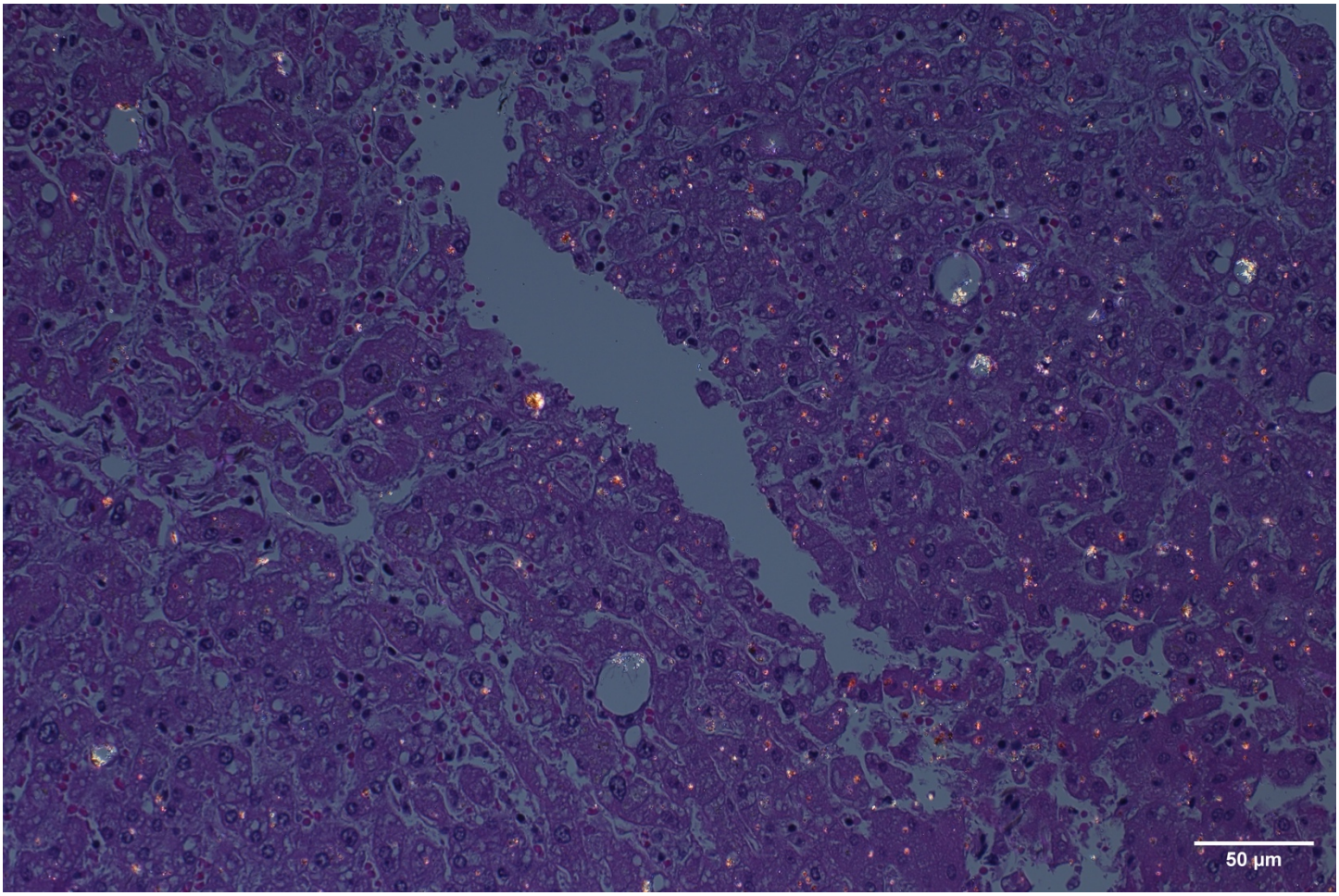

Figure S7. Representative polarization wave imaging of the liver (hematoxylin and eosin staining), revealing the widespread nature of refractory inclusions. Sections from 12 subjects were examined.

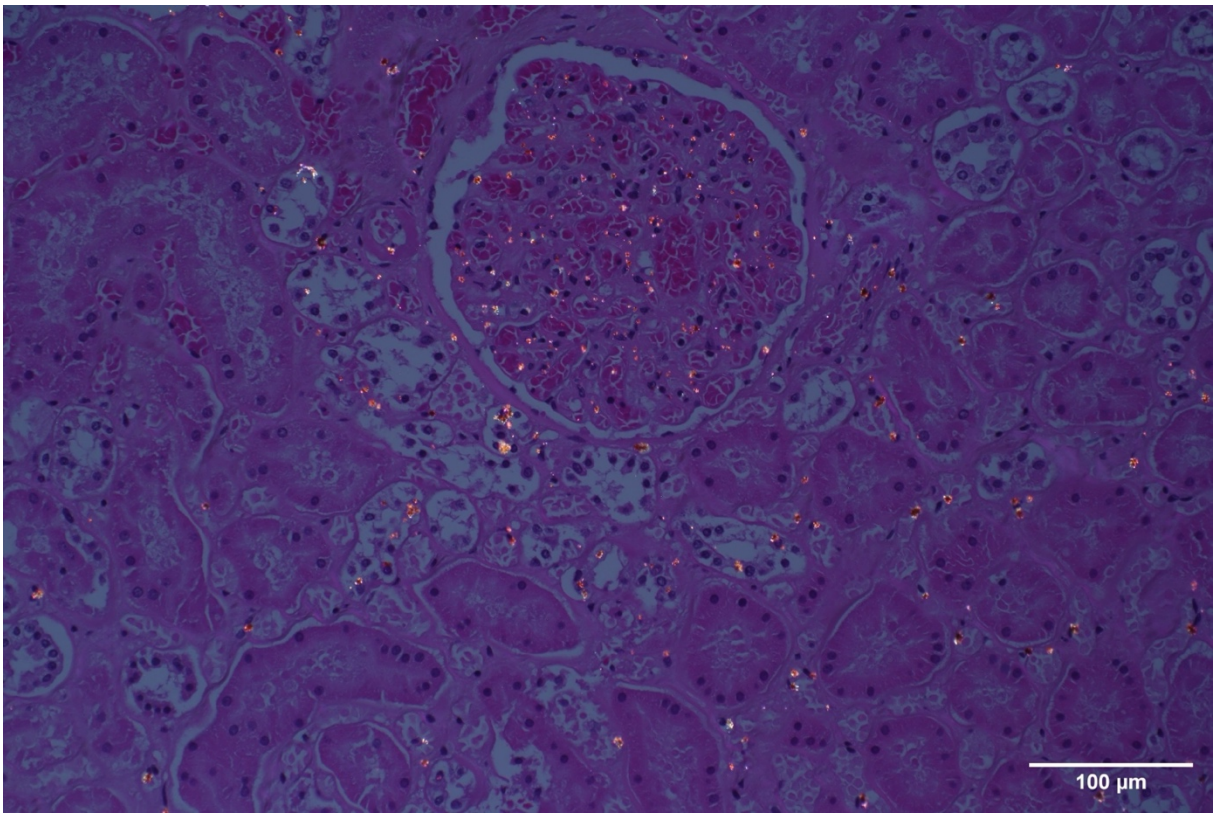

Figure S8. Polarization wave imaging of the kidney (hematoxylin and eosin staining), revealing the widespread nature of refractory inclusions. Sections from 12 subjects were examined.

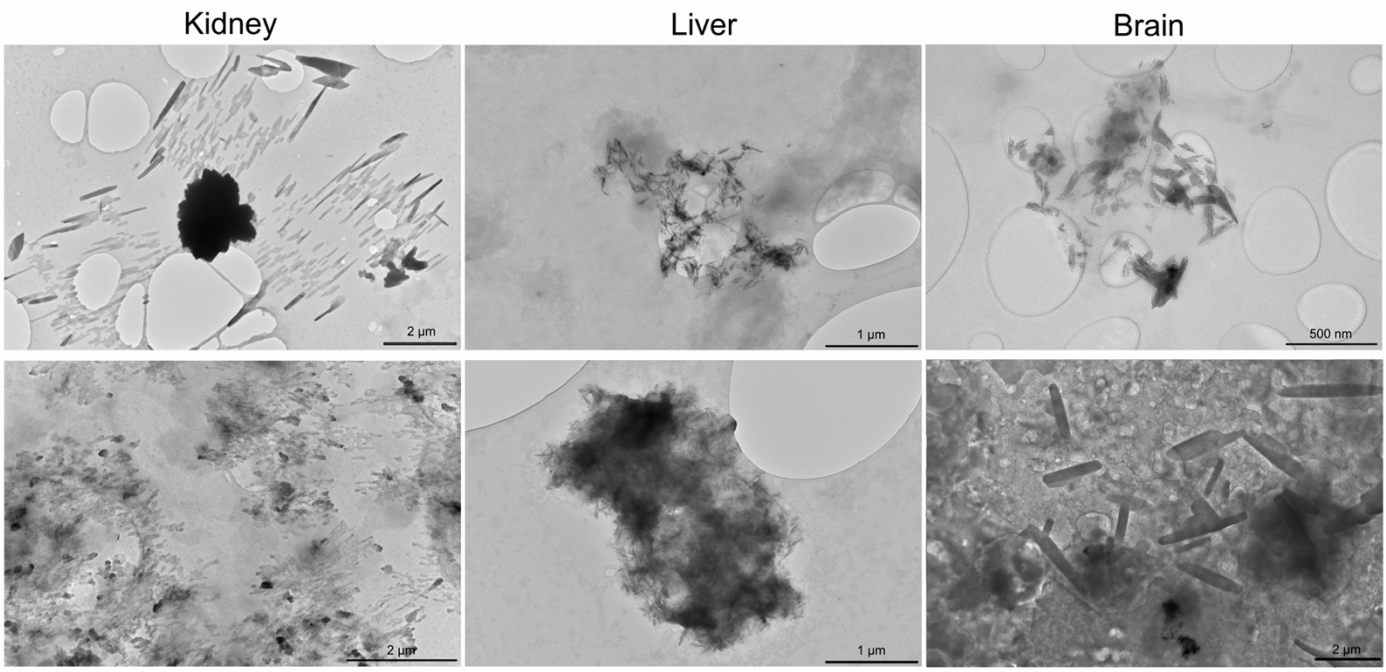

Figure S9. Additional representative TEM images of isolated, dispersed particulates from the liver, kidney, and brain pellets that were used for Py-GC/MS. Pellets from 3 subjects for each organ have been imaged by TEM.

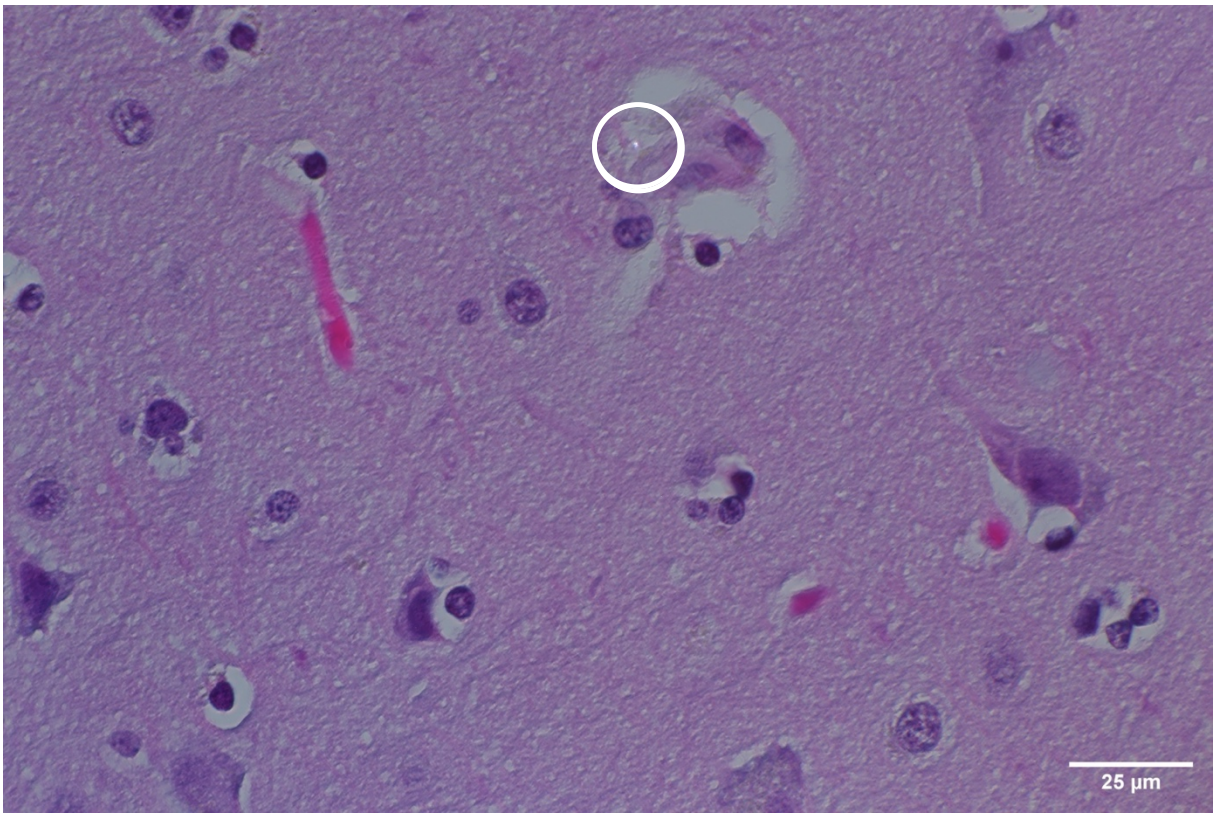

Figure S10. Polarization wave imaging of the brain (hematoxylin and eosin staining), revealing refractory inclusions (circled) visible with light microscopy. Sections from 10 subjects were examined.

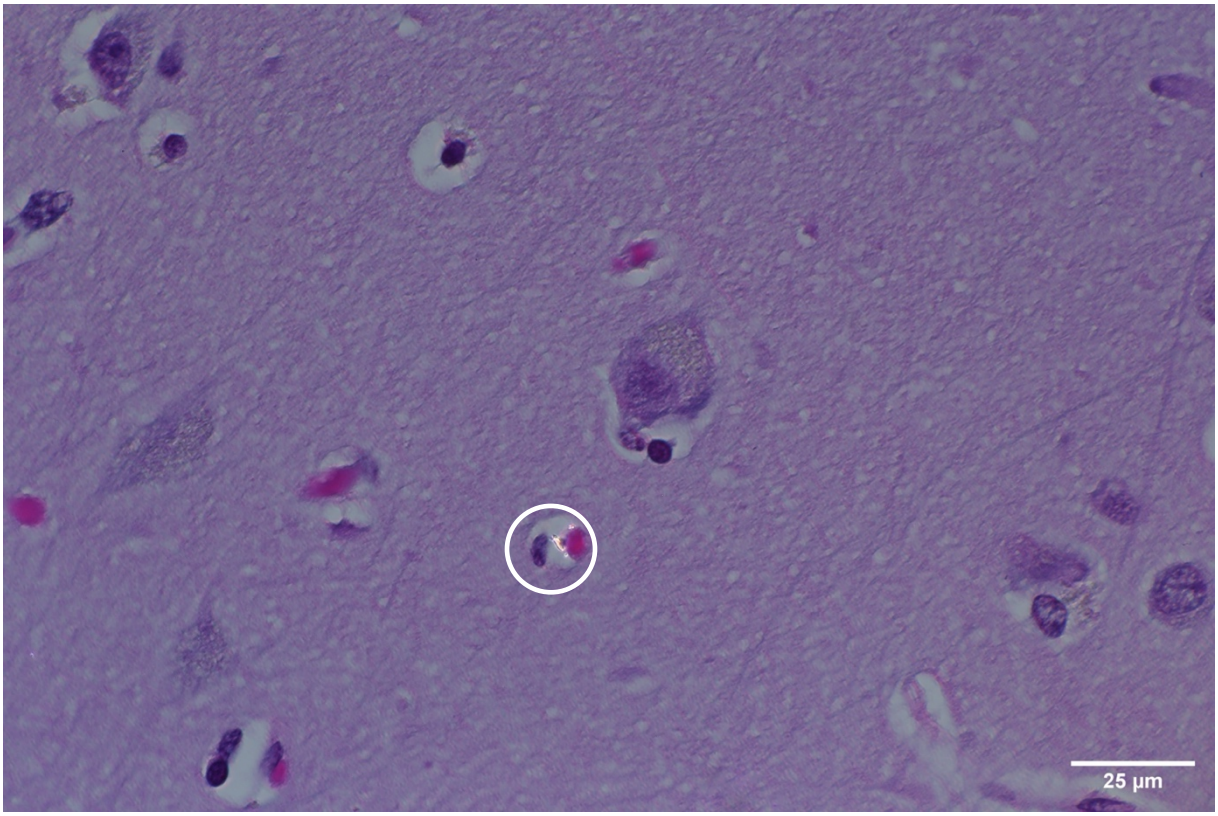

Figure S11. Polarization wave imaging of the brain (hematoxylin and eosin staining), revealing refractory inclusions (circled) visible with light microscopy. Sections from 10 subjects were examined.

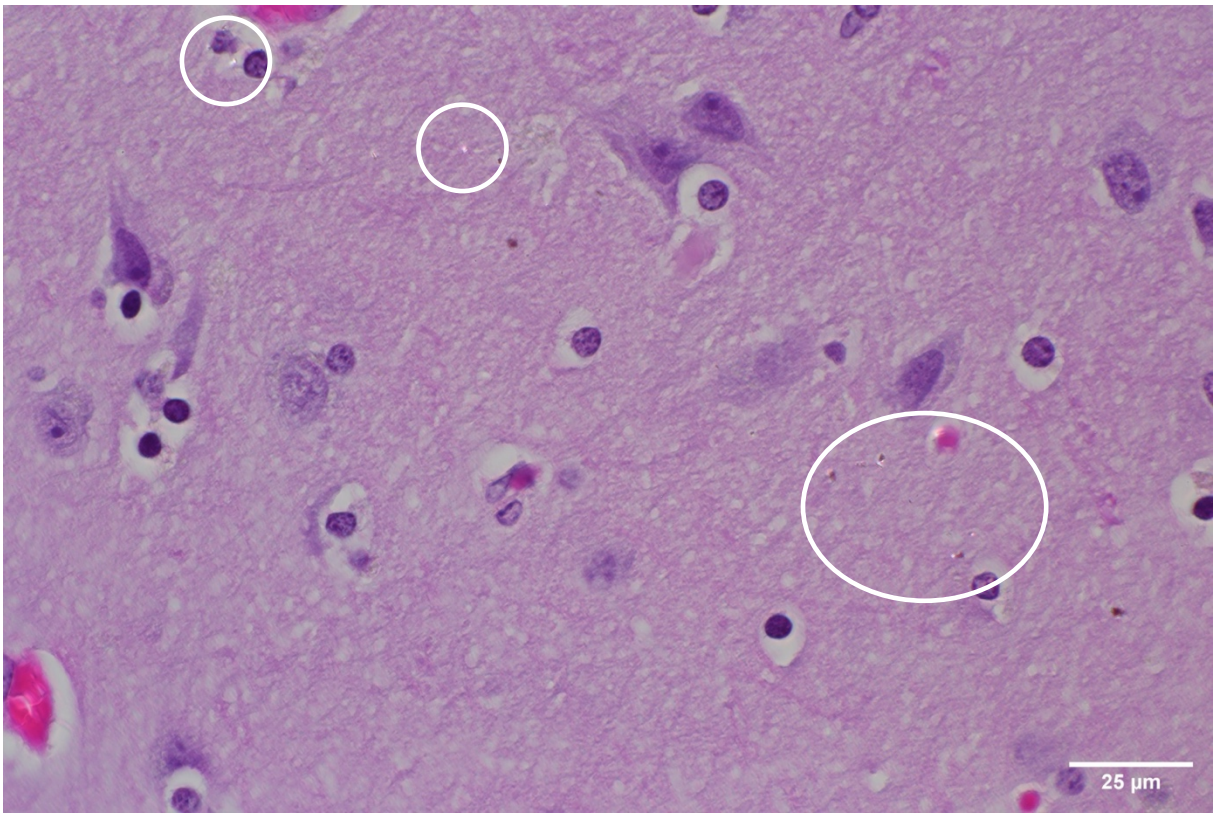

Figure S12. Polarization wave imaging of the brain (hematoxylin and eosin staining), revealing refractory inclusions (circled) visible with light microscopy. Sections from 10 subjects were examined.

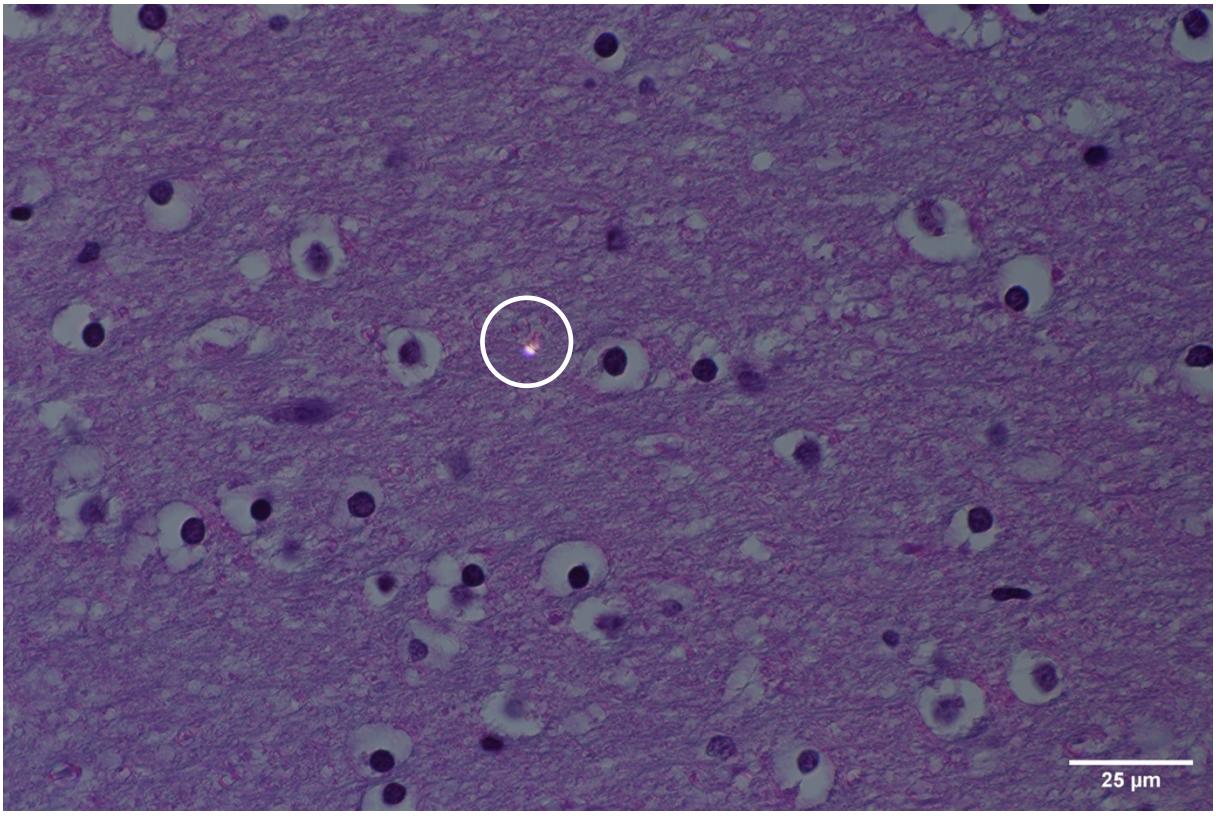

Figure S13. Polarization wave imaging of the brain (hematoxylin and eosin staining), revealing refractory inclusions (circled) visible with light microscopy. Sections from 10 subjects were examined.

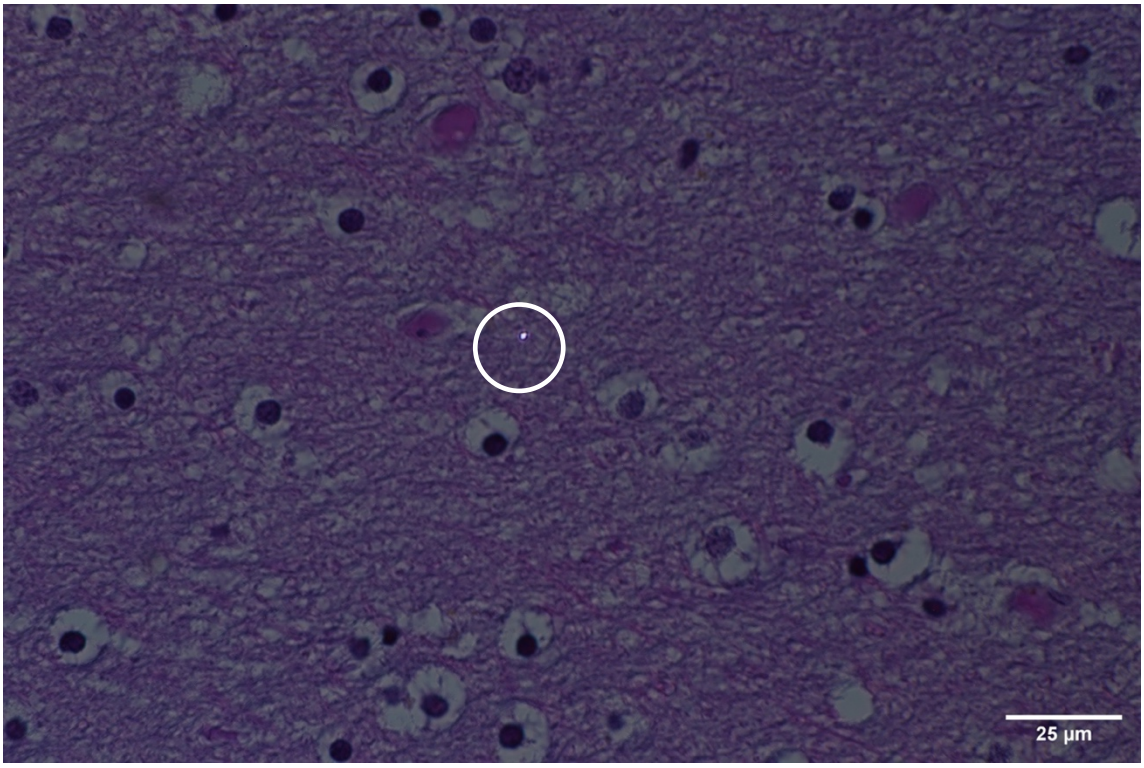

Figure S14. Polarization wave imaging of the brain (hematoxylin and eosin staining), revealing refractory inclusions (circled) visible with light microscopy. Sections from 10 subjects were examined.

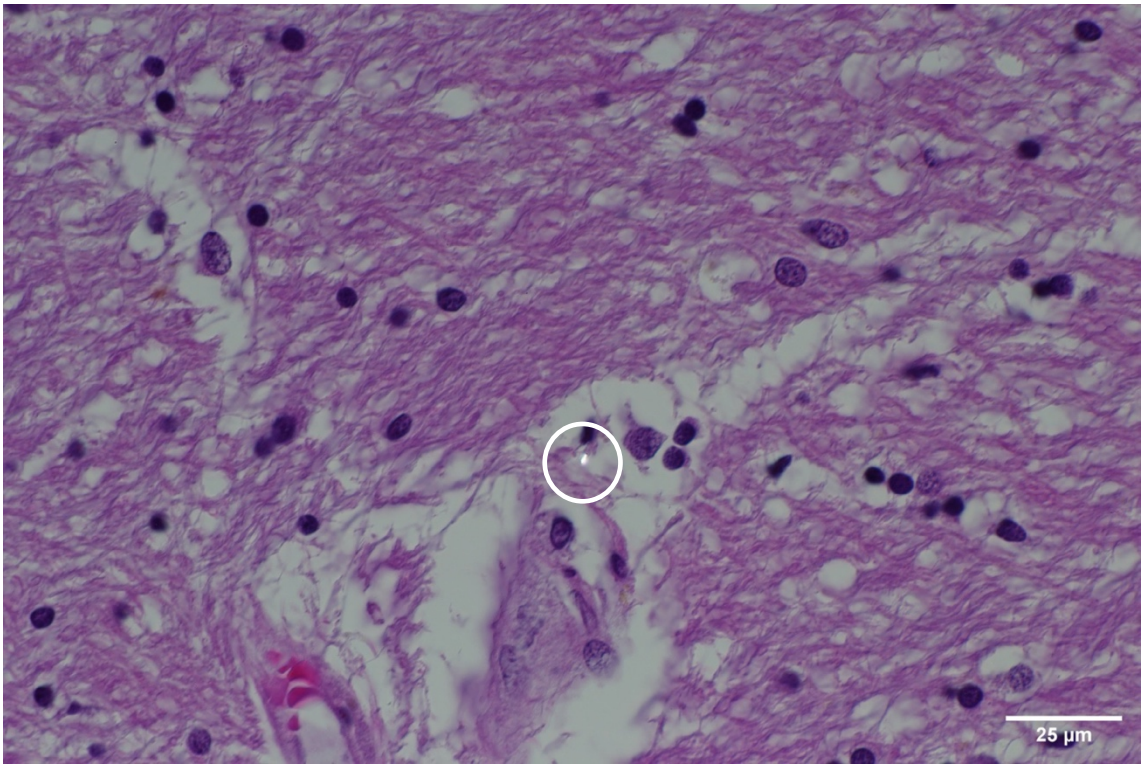

Figure S15. Polarization wave imaging of the brain (hematoxylin and eosin staining), revealing refractory inclusions (circled) visible with light microscopy. Sections from 10 subjects were examined.

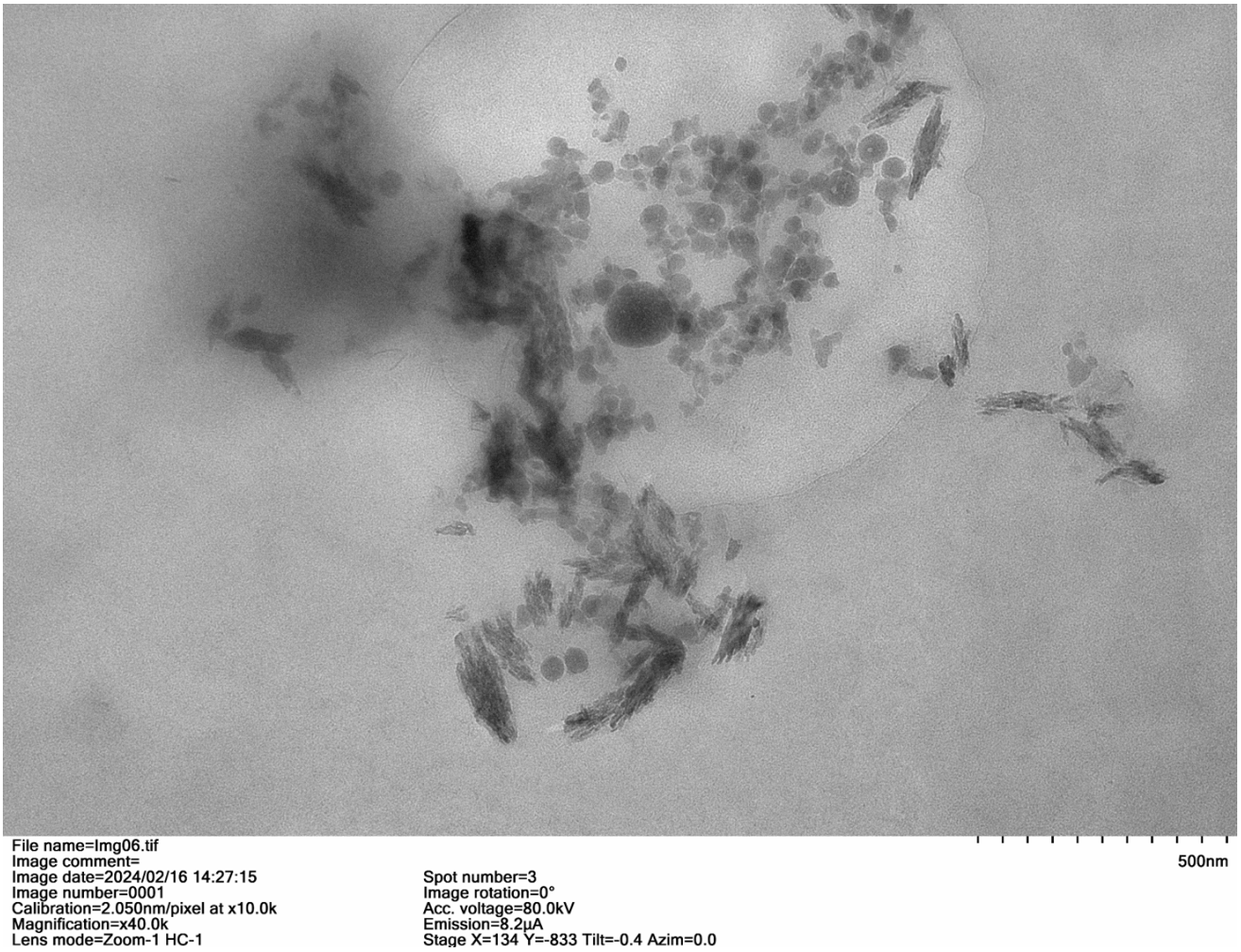

Figure S16. TEM image of particles from an isolated pellet derived from a human decedent brain, illustrating numerous particulates smaller than 200 nm in length/diameter. This image reveals some of the diversity of shapes present, although most appeared to be shard-like fragments. Representative image taken from a single pellet.

2.2. Nile Red Staining

The mass and aliquots for sample preparation of the pellets for instrumentation can be found in Table S11. Total particle numbers including individual particles, fibers, and fragments can be found in Table S12. Imaging of stereoscope and Nile Red can be found in Figures S17-S19.

2.3. FTIR Reflectance Analysis

FTIR reflectance results can be found in Table S13. Automated FTIR reflectance imaging can be found in Figure S17. Overall, all polymers matched in all five samples with the in-house library of the instrument. The specific type of polymer is indicated as the highest match of the library selection per point. Copolymer matches (e.g., polyethylene:propylene:diene) were identified in all five samples. The highest match above 60% was chosen for reporting, however, in some cases individual polymers were found at a lower match and varying polymer libraries based on the collected spectra (individual data not provided). Therefore, the specific type of polymer being reported from the copolymer may need further consideration. Regardless, the presence of plastics was both visually and analytically

confirmed for the samples and reinforces the presence of multiple polymer and copolymer types in the samples (Figure S19).

2.4. ATR-FTIR Analysis

Individual particles analyzed for ATR-FTIR can be found in Table S13 and examples of the particles assessed shown in Figures S20-S25. Polymers that matched above 60% were only found in three samples (B1, B3, and B5) with rayon being measured in all 3. Results where polymers were measured at less than 60% may be an issue with the small size of the particles and possibly the residual post-digestion biomatrix. Samples that were around 20 µm or less will result in reduced sensitivity of the spectra analysis as this is the minimum threshold for sensitivity of the instrument; such large particles were infrequently observed in brain-derived samples. Therefore, the polymer spectra may have increased matching accuracy with increased particle size. However, both mosaic heat mapping and ATR-FTIR confirmed the presence of some polymers in the samples.

2.5. Py-GC/MS Analysis (OSU)

Mass of the Py-GC/MS measured at OSU can be found in Table S15, with numbers expressed relative to the pellet weight, but not to the tissue sample weight (as in Figure 1 of the main manuscript). Results indicated polymers in each sample aliquot. Polyethylene (PE) was the highest concentration found in all 5 samples followed by Nylon 66 (N66), acrylonitrile butadiene styrene (ABS) and polyethylene terephthalate (PET). Polyvinyl chloride (PVC) was detected only in Sample B1 and styrene-butadiene rubber (SBR) was found only in sample B5. Sample 4 had the lowest concentration of the majority of polymers, however the sample size should be considered for reporting. The concentrations found in the samples reinforce results of heatmapping reflectance where the abundance of plastic spectra identified were similar plastic types found by Py-GC/MS. Moreover, the number of points identified as polymers with reflectance specific to the individual samples, highlights the concentrations found in Py-GC/MS (*i.e.*, sample B4 having lower detection points and concentrations and with samples B1-3 having higher points and concentrations).

Table S11. Sample mass of tissue pellets and aliquots for Py-GC-MS.

Sample ID	Initial Pellet (mg)	Replicate	Aliqout (mg)
B1	4.975	1	1.17
		2	1.427
B2	5.18	1	1.375
		2	1.235
B3	9.588	1	1.159
		2	1.456
		3	1.244
B4	2.766	1	1.045
B5	9.488	1	1.041
		2	1.038
		3	1.612

Table S12. Particles numbers detected and identified with Nile Red using fluorescence.

Sample Number	Average Particles Quantified	Average Particle Type
B1	63	3 fibers
		7 fragments
		53 particles
B2	186	2 fibers
		20 fragments
		164 particles
B3	502	6 fibers
		66 fragments
		430 particles
B4	119	3 fibers
		21 fragments
		95 particles
B5	122	3 fibers
		19 fragments
		100 particles
Blank	25	0 fibers
		1.7 fragments
		24 particles

Table S13. Particles detected and identified with FTIR reflectance and spectra analysis of individual points.

Sample Number	ATR Particle Tag	Particle Type	Match (%)
B1	B1-Heat 1	Rayon	50.05
	B1-Heat 2	Poly(Vinyl Butyral)	46.79
	B1-Heat 3	Poly(Ethylene: Propylene: Diene)	85.86
	B1-Heat 4	Poly(Ethylene: Propylene: Diene)	67.14
	B1-Heat 5	Poly(Ethylene: Propylene: Diene)	80.69
	B1-Heat 6	Poly(Ethylene: Propylene: Diene)	93.51
	B1-Heat 7	Poly(Ethylene: Propylene: Diene)	93.9
	B1-Heat 8	Poly(Ethylene: Propylene: Diene)	79.45
	B1-Heat 9	Poly(Ethylene: Propylene: Diene)	79.58
	B1-Heat 10	Poly(Ethylene: Propylene: Diene)	82.31
	B1-Heat 11	Poly(Ethylene: Propylene: Diene)	91.92
	B1-Heat 12	Poly(Ethylene: Propylene: Diene)	85.96
	B1-Heat 13	Poly(Ethylene: Propylene: Diene)	91.81
	B1-Heat 14	Poly(Ethylene: Propylene: Diene)	85.97
B2	B2-Heat 1	Poly(Ethylene: Propylene: Diene)	86.03
	B2-Heat 2	Rayon	45.65
	B2-Heat 3	Silicon Dioxide	43.06
	B2-Heat 4	Nylon	65.98
	B2-Heat 5	Poly(Ethylene: Propylene: Diene)	89.31
	B2-Heat 6	Poly(Ethylene: Propylene: Diene)	70.92
	B2-Heat 7	Poly(Ethylene: Propylene: Diene)	46.11
	B2-Heat 8	LDPE	45.52
	B2-Heat 9	Polyoxyethylene Isodecyl Ether Phosphate	39.02
	B2-Heat 10	Poly(styrene), Actacic	60.74
B3	B3-Heat 1	Poly(Ethylene: Propylene: Diene)	92.83
	B3-Heat 2	Poly(Ethylene: Propylene: Diene)	87.82
	B3-Heat 3	Poly(Ethylene: Propylene: Diene)	89.61
	B3-Heat 4	Poly(Ethylene:Vinyl Chlroide)	71.88
	B3-Heat 5	Olefin	79.75
	B3-Heat 6	Poly(Ethylene: Propylene)	82.07
	B3-Heat 7	Poly(Ethylene:Vinyl Chlroide)	72.56
	B3-Heat 8	Olefin	77.78
	B3-Heat 9	Poly(Ethylene: Propylene: Diene)	96.02
	B3-Heat 10	Poly(Ethylene: Propylene)	92.66
	B3-Heat 11	Poly(Ethylene: Propylene)	76.41
	B3-Heat 12	Poly(Ethylene: Propylene)	79.58
	B3-Heat 13	Poly(Ethylene:Vinyl Chlroide)	42.72
	B3-Heat 14	Poly(Ethylene: Propylene)	57.76

Sample Number	Particle Tag	Particle Type	Match (%)
B1	B1-Heat 1	Rayon	50.05
	B1-Heat 2	Poly(Vinyl Butyral)	46.79
	B1-Heat 3	Poly(Ethylene: Propylene: Diene)	85.86
	B1-Heat 4	Poly(Ethylene: Propylene: Diene)	67.14
	B1-Heat 5	Poly(Ethylene: Propylene: Diene)	80.69
	B1-Heat 6	Poly(Ethylene: Propylene: Diene)	93.51
	B1-Heat 7	Poly(Ethylene: Propylene: Diene)	93.9
	B1-Heat 8	Poly(Ethylene: Propylene: Diene)	79.45
	B1-Heat 9	Poly(Ethylene: Propylene: Diene)	79.58
	B1-Heat 10	Poly(Ethylene: Propylene: Diene)	82.31
	B1-Heat 11	Poly(Ethylene: Propylene: Diene)	91.92
	B1-Heat 12	Poly(Ethylene: Propylene: Diene)	85.96
	B1-Heat 13	Poly(Ethylene: Propylene: Diene)	91.81
	B1-Heat 14	Poly(Ethylene: Propylene: Diene)	85.97
B2	B2-Heat 1	Poly(Ethylene: Propylene: Diene)	86.03
	B2-Heat 2	Rayon	45.65
	B2-Heat 3	Silicon Dioxide	43.06
	B2-Heat 4	Nylon	65.98
	B2-Heat 5	Poly(Ethylene: Propylene: Diene)	89.31
	B2-Heat 6	Poly(Ethylene: Propylene: Diene)	70.92
	B2-Heat 7	Poly(Ethylene: Propylene: Diene)	46.11
	B2-Heat 8	LDPE	45.52
	B2-Heat 9	Polyoxyethylene Isodecyl Ether Phosphate	39.02
	B2-Heat 10	Poly(styrene), Actacic	60.74
B3	B3-Heat 1	Poly(Ethylene: Propylene: Diene)	92.83
	B3-Heat 2	Poly(Ethylene: Propylene: Diene)	87.82
	B3-Heat 3	Poly(Ethylene: Propylene: Diene)	89.61
	B3-Heat 4	Poly(Ethylene:Vinyl Chlroide)	71.88
	B3-Heat 5	Olefin	79.75
	B3-Heat 6	Poly(Ethylene: Propylene)	82.07
	B3-Heat 7	Poly(Ethylene:Vinyl Chlroide)	72.56
	B3-Heat 8	Olefin	77.78
	B3-Heat 9	Poly(Ethylene: Propylene: Diene)	96.02
	B3-Heat 10	Poly(Ethylene: Propylene)	92.66
	B3-Heat 11	Poly(Ethylene: Propylene)	76.41
	B3-Heat 12	Poly(Ethylene: Propylene)	79.58
	B3-Heat 13	Poly(Ethylene:Vinyl Chlroide)	42.72
	B3-Heat 14	Poly(Ethylene: Propylene)	57.76

B4	B3-Heat 15	Poly(Ethylene: Propylene: Diene)	67.79
	B3-Heat 16	Rayon	49.48
	B3-Heat 17	Talc Powder	64.47
	B3-Heat 18	Aluminum 2,9,16,23-Tetraphenyl-29H,31H-Phthalocyanine Chloride	61.25
	B3-Heat 19	Olefin	72.71
	B3-Heat 20	Olefin	77.18
	B3-Heat 21	Olefin	72.56
	B3-Heat 22	Poly(Ethylene: Propylene: Diene)	83.89
	B3-Heat 23	Rayon	51.14
	B3-Heat 24	Poly(Ethylene: Propylene: Diene)	74.8
	B3-Heat 25	Rayon	54.66
	B3-Heat 26	Tributyl Phosphate	45.7
	B3-Heat 27	Trimethyl Phosphite	50.44
	B3-Heat 28	LDPE	59.66
B5	B3-Heat 29	Poly(Vinyl Chloride:Ethylene)	50.94
	B3-Heat 30	Poly(Ethylene:Vinyl Chlroide)	69.72
	B3-Heat 31	Polystyrene	55.45
	B3-Heat 32	Poly(Ethylene: Propylene: Diene)	72.64
	B3-Heat 33	Poly(Ethylene: Propylene: Diene)	63.56
	B3-Heat 34	Rayon	40.02
	B3-Heat 35	Poly(Ethylene: Propylene: Diene)	91.96
	B3-Heat 36	Rayon	36.68
	B3-Heat 37	Poly(Ethylene:Vinyl Chlroide)	70.42
	B3-Heat 38	Rayon	59.58
	B3-Heat 39	Poly(Ethylene: Propylene: Diene)	73.89
	B3-Heat 40	Poly(Ethylene: Propylene: Diene)	79.31
	B3-Heat 41	Poly(Ethylene: Propylene: Diene)	87.09
	B3-Heat 42	Poly(Ethylene: Propylene: Diene)	90.53
Blank	B3-Heat 43	2,2'-Sulfonyldiethanol	34.34
	B3-Heat 44	Polyphenylene Oxide	49.05
	B3-Heat 45	Ethyl Nitrite	54.64
	B3-Heat 46	Butyl Sulfone	44.72
	B3-Heat 47	Polyethylene teraphalate	40.49
	B3-Heat 48	Zirconium(IV) Propoxide	28.8
	B3-Heat 49	Ethyl-1,1-D2 Alcohol	33.92
	B3-Heat 50	Cadmium, Zinc, Barium Sulfide Blend	63.9
	B3-Heat 51	2,6-Naphthalenedisulfonic Acide, Disodium Salt	28.97
	B3-Heat 52	3,4-Epoxytetrahydrothiophene-1,1-Dioxide	35.71
	B3-Heat 53	Ethylene Diamine Phosphate	34.28
	B3-Heat 54	1,3-Dichloro-1,1,3,3-Tetraisopropyldisiloxane	34.55
	B3-Heat 55	Ethyl-2,2,2-D3 Alcohol	35.01
	B3-Heat 56	2-Hydroxyethyl Disulfide	39.76

B4	B4-Heat 1	Poly(Ethylene: Propylene: Diene)	67.79
	B4-Heat 2	Rayon	49.48
	B4-Heat 3	Talc Powder	64.47
	B4-Heat 4	Aluminum 2,9,16,23-Tetraphenyl-29H,31H-Phthalocyanine Chloride	61.25
	B4-Heat 5	Olefin	72.71
	B4-Heat 6	Olefin	77.18
	B4-Heat 7	Olefin	72.56
	B4-Heat 8	Poly(Ethylene: Propylene: Diene)	83.89
	B4-Heat 9	Rayon	51.14
	B4-Heat 10	Poly(Ethylene: Propylene: Diene)	74.8
	B4-Heat 11	Rayon	54.66
	B4-Heat 12	Tributyl Phosphate	45.7
	B4-Heat 13	Trimethyl Phosphite	50.44
	B4-Heat 14	LDPE	59.66
B5	B5-Heat 1	Poly(Vinyl Chloride:Ethylene)	50.94
	B5-Heat 2	Poly(Ethylene:Vinyl Chlroide)	69.72
	B5-Heat 3	Polystyrene	55.45
	B5-Heat 4	Poly(Ethylene: Propylene: Diene)	72.64
	B5-Heat 5	Poly(Ethylene: Propylene: Diene)	63.56
	B5-Heat 6	Rayon	40.02
	B5-Heat 7	Poly(Ethylene: Propylene: Diene)	91.96
	B5-Heat 8	Rayon	36.68
	B5-Heat 9	Poly(Ethylene:Vinyl Chlroide)	70.42
	B5-Heat 10	Rayon	59.58
	B5-Heat 11	Poly(Ethylene: Propylene: Diene)	73.89
	B5-Heat 12	Poly(Ethylene: Propylene: Diene)	79.31
	B5-Heat 13	Poly(Ethylene: Propylene: Diene)	87.09
	B5-Heat 14	Poly(Ethylene: Propylene: Diene)	90.53
Blank	Blank-Heat 1	2,2'-Sulfonyldiethanol	34.34
	Blank-Heat 2	Polyphenylene Oxide	49.05
	Blank-Heat 3	Ethyl Nitrite	54.64
	Blank-Heat 4	Butyl Sulfone	44.72
	Blank-Heat 5	Polyethylene teraphalate	40.49
	Blank-Heat 6	Zirconium(IV) Propoxide	28.8
	Blank-Heat 7	Ethyl-1,1-D2 Alcohol	33.92
	Blank-Heat 8	Cadmium, Zinc, Barium Sulfide Blend	63.9
	Blank-Heat 9	2,6-Naphthalenedisulfonic Acide, Disodium Salt	28.97
	Blank-Heat 10	3,4-Epoxytetrahydrothiophene-1,1-Dioxide	35.71
	Blank-Heat 11	Ethylene Diamine Phosphate	34.28
	Blank-Heat 12	1,3-Dichloro-1,1,3,3-Tetraisopropyldisiloxane	34.55
	Blank-Heat 13	Ethyl-2,2,2-D3 Alcohol	35.01
	Blank-Heat 14	2-Hydroxyethyl Disulfide	39.76

Table S14. The number of particles detected and identified with ATR-FTIR, including the particle type and percentage matches. Images corresponding to these results are shown in figures S20-S24 for samples B1-B5, respectively.

Sample Number	FTIR Particle Tag	Particle Type	Match (%)
B1	B1-Point 1	Rayon	77.88
	B1-Point 2	(2,2'-Bipyridine) Dichloroopalladium(II))	40.06
	B1-Point 3	Endothermic Foaming Agent #2	40.76
	B1-Point 4	Trans, Trans Benzaldehyde Azine	38.26
	B1-Point 5	Rayon	26.5
	B1-Point 6	1,4-Diphenylbutadiyne	35.33
	B1-Point 7	Trans, Trans Benzaldehyde Azine	38.93
	B1-Point 8	Polyester	32.06
	B1-Point 9	Rayon	50.29
	B1-Point 10	Polypropylene	95.2
B2	B2-Point 1	Polystyrene	49.25
	B2-Point 2	Poly(Vinylidnene) Fluoride	25.61
	B2-Point 3	Fluorotriphenyltin	31.53
	B2-Point 4	Poly(Styrene), Actactic	36.72
	B2-Point 5	Poly(Styrene:Vinylidene Chloride)	35.2
	B2-Point 6	Rayon	27.24
	B2-Point 7	Polyethylene	36.39
	B2-Point 8	LDPE	45.52
	B2-Point 9	Polystyrene	38.24
	B2-Point 10	N,N' Ethylene Bis Stearamide	87.08
B3	B3-Point 1	Poly(Styrene), Actactic	43.69
	B3-Point 2	Rayon	73.23
	B3-Point 3	LDPE	47.57
	B3-Point 4	Olefin	43.89
	B3-Point 5	Azobenzene	37.14
	B3-Point 6	Polystyrene	27.16
	B3-Point 7	Polystyrene	39.79
	B3-Point 8	LDPE	31.4
	B3-Point 9	Polystyrene	49.45
	B3-Point 10	2-Chloroethyl Methyl Sulfide	36.3

B4	B4-Point 1	Tetraphenyltin	27.46
	B4-Point 2	Polystyrene	48.64
	B4-Point 3	Poly(Styrene), Actactic	50.28
	B4-Point 4	Polystyrene	51.93
	B4-Point 5	Polyethylene Maleic Copolymer	27.35
	B4-Point 6	Rayon	45.64
	B4-Point 7	Benzyl Sulfone	35.07
	B4-Point 8	Phenylthiocopper	34.69
	B4-Point 9	Polystyrene	41.84
	B4-Point 10	(+)-(S)-N,N-Dimethyl-1-((R)-2-(Diphenylphosphino)Ferrocenyl	30.3
B5	B5-Point 1	Polyethylene	36.4
	B5-Point 2	Rayon	60.87
	B5-Point 3	LDPE	53.88
	B5-Point 4	Polstyrene	55.59
	B5-Point 5	Tetrabutylammonium Difluorotriphenylstannate	28.68
	B5-Point 6	N-Benzylidnene-4-Chlroaniline	27.45
	B5-Point 7	Ammonium Fluoralkyl Sulfonate	41.29
	B5-Point 8	Polystyrene	59.44
	B5-Point 9	Tetraphenylarsonium Chloride Hydrate	32.58
	B5-Point 10	Benzyltriphenyltin	44.25
Blank	B5-Point 1	Polystyrene	39.45

Table S15. Polymer concentrations measured by Py-GC/MS (relative to pellet weight, not original tissue sample). Results are presented as average ± standard deviation. Samples were repeated in triplicate unless otherwise notated: * Indicates sample size of n = 1; ** Indicates sample size of n = 2.

Sample	Ave ± SD Concentration of Polymer (µg/mg)					
	PE	N66	ABS	PET	PVC	SBR
Brain 1	33.5 ± 7.29**	4.20 ± 0.78**	0.26 ± 0.03**	0.09 ± 0.02**	0.03 ± 0.04**	ND
Brain 2	32.0± 13.3**	3.77 ± 0.29**	0.21 ± 0.03**	0.07*	ND	ND
Brain 3	36.67 ± 13.87	3.53 ± 0.54	0.15 ± 0.12	0.07 ± 0.01	ND	ND
Brain 4	17.0*	1.01*	0.02*	0.07*	ND	ND
Brain 5	27.4 ± 2.72	3.34 ± 0.17	0.26 ± 0.06	0.08 ± 0.02	ND	1.06*

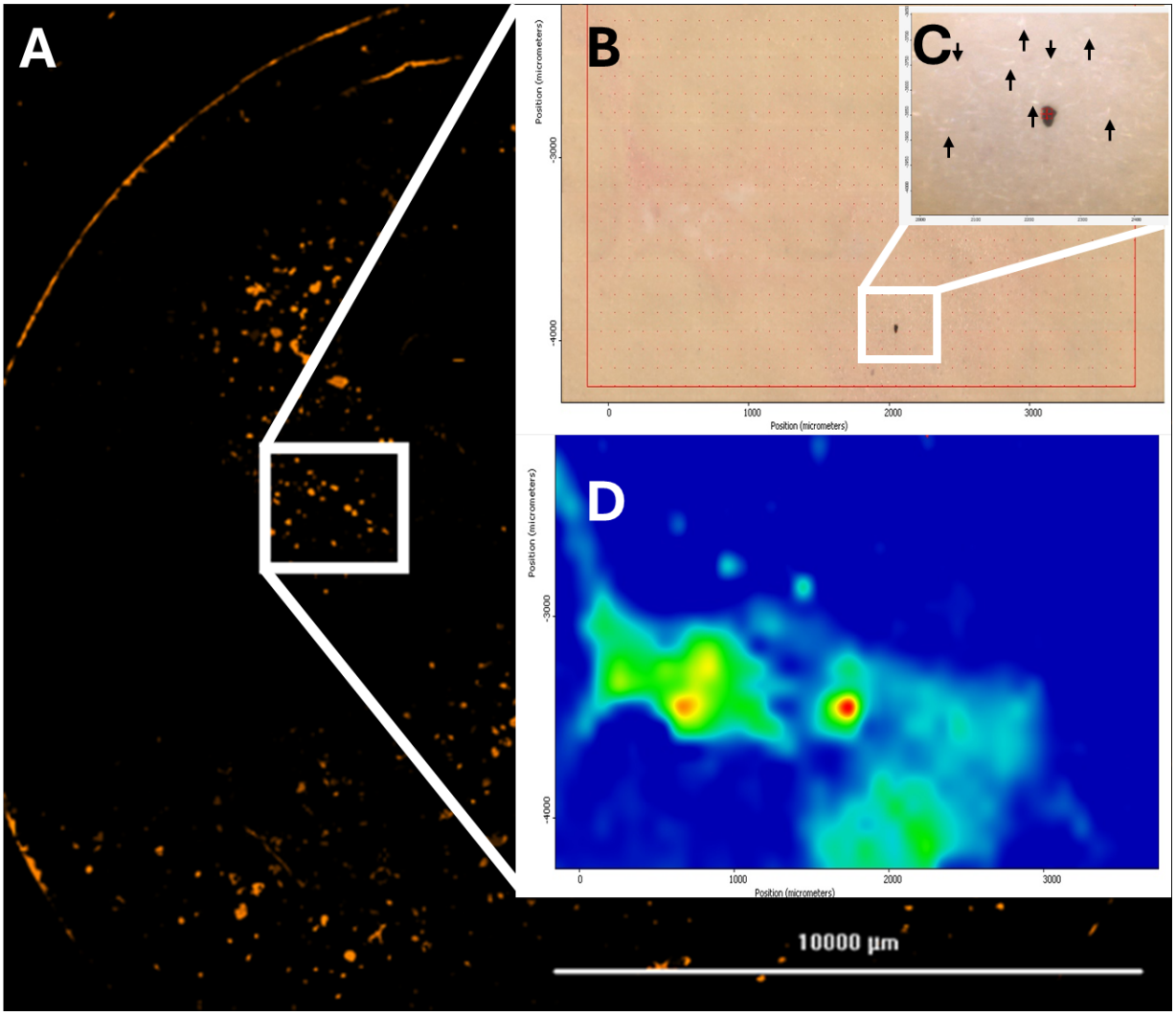

Figure S17. Particle imaging of human brain tissue using Nile Red staining with fluorescence (A). FTIR mosaic mapping (B) was used to visually inspect particles indicated with arrows (C). Particle types were confirmed using FTIR mapping (D).

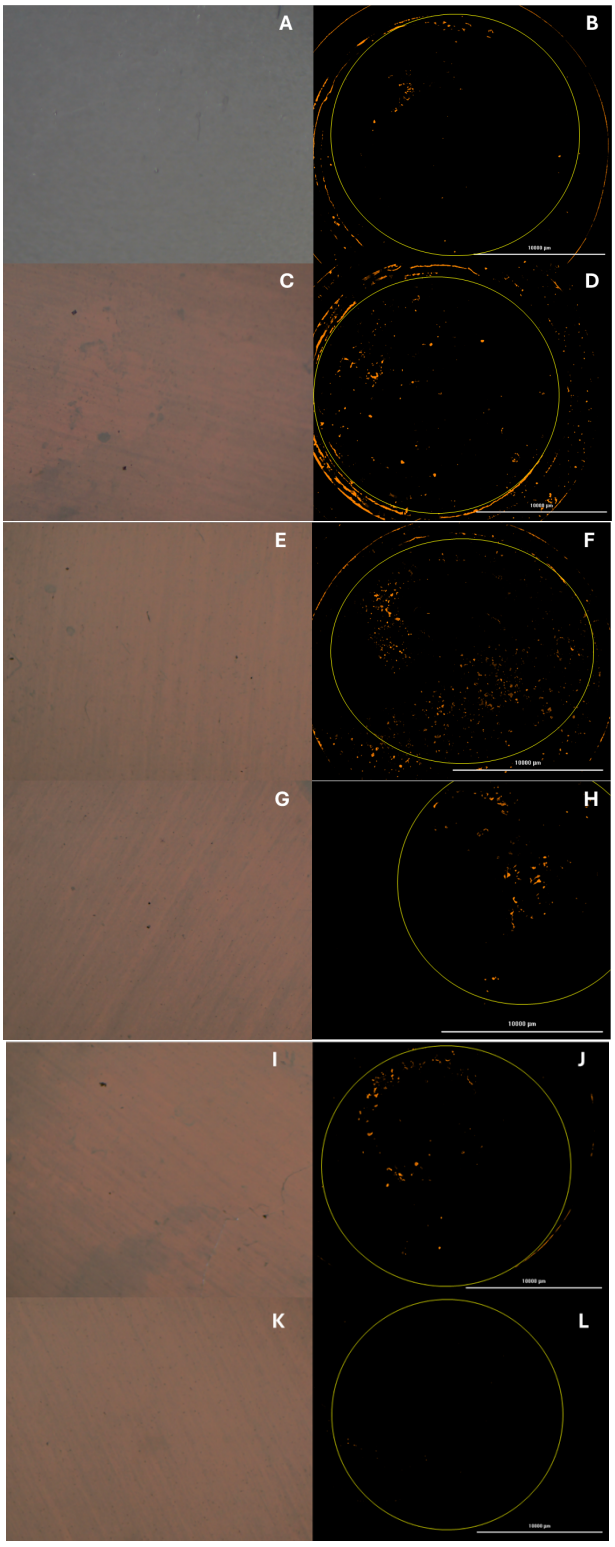

Figure S18. Sample B1 stereomicroscope (A) and Nile Red fluorescently stained (B) particle images. Sample B2 stereomicroscope (C) and Nile Red fluorescently stained (D) particle images. Sample B3 stereomicroscope (E) and Nile Red fluorescently stained (F) particle images. Sample B4 stereomicroscope (G) and Nile Red fluorescently stained (H) particle images. Sample B5 stereomicroscope (I) and Nile Red fluorescently stained (J) particle images. Control sample stereomicroscope (K) and Nile Red fluorescently stained (L) particle images. The yellow circle demonstrates the filter area that was selected for particle quantification.

Figure S19. Sample B1 mosaic image (A) and mapping (B) particle images. Sample B2 B1 mosaic image (C) and mapping (D) particle images. Sample B3 mosaic image (E) and mapping (F) particle images. Sample B4 mosaic image (G) and mapping (H) particle images. Sample B5 mosaic image (I) and mapping (J) particle images. Control sample mosaic image (K) and mapping (L) particle images. Numbers and arrows indicate analyzed particle spectra found in Table S9.

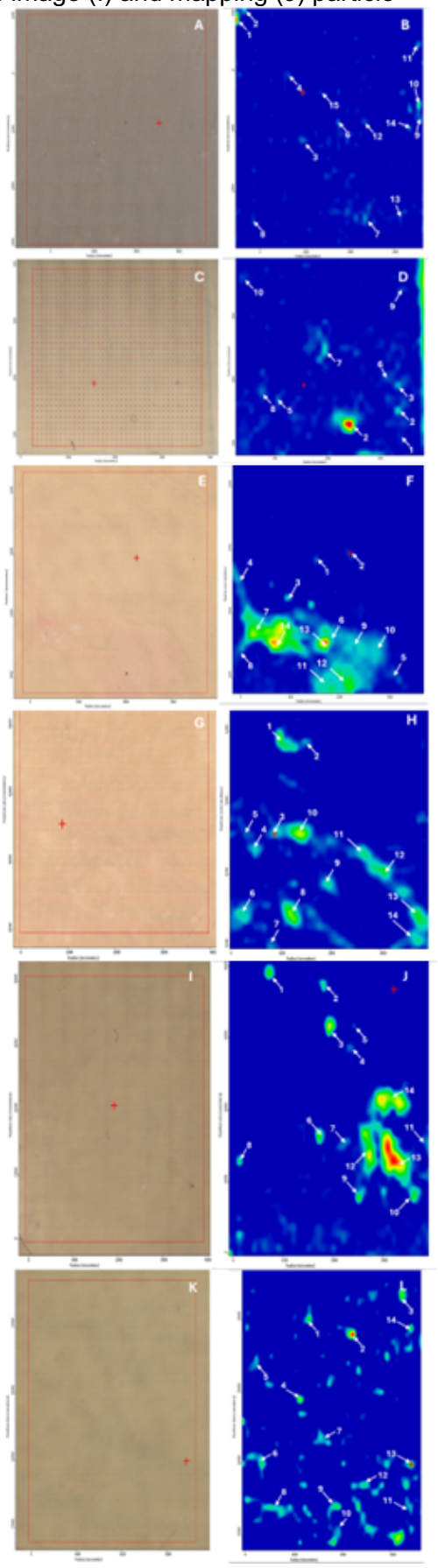

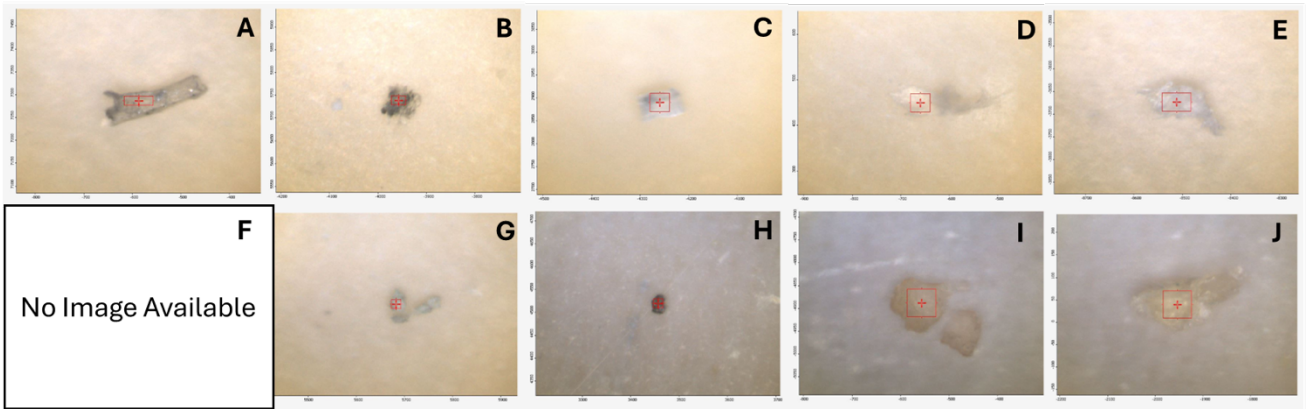

Figure S20. ATR-FTIR particle selection for sample B1.

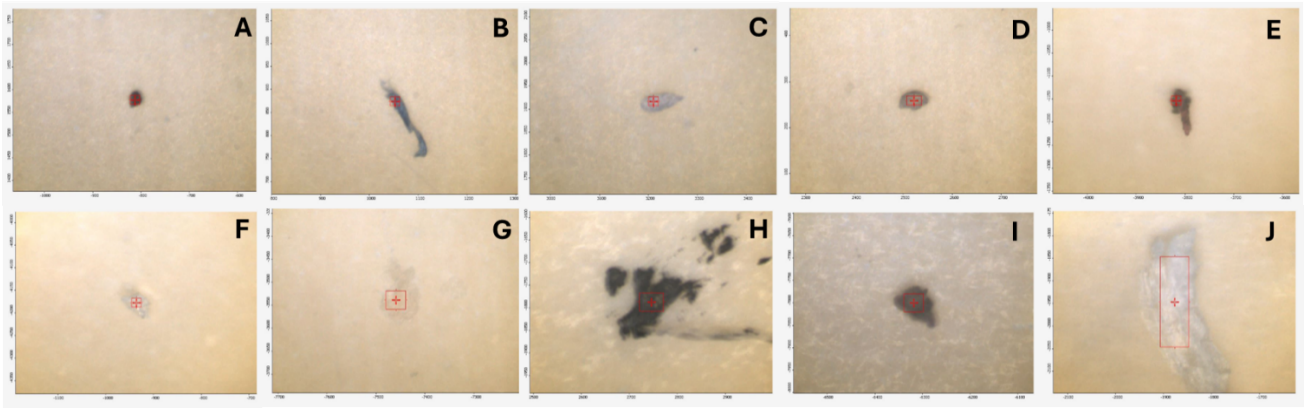

Figure S21. ATR-FTIR particle selection for sample B2.

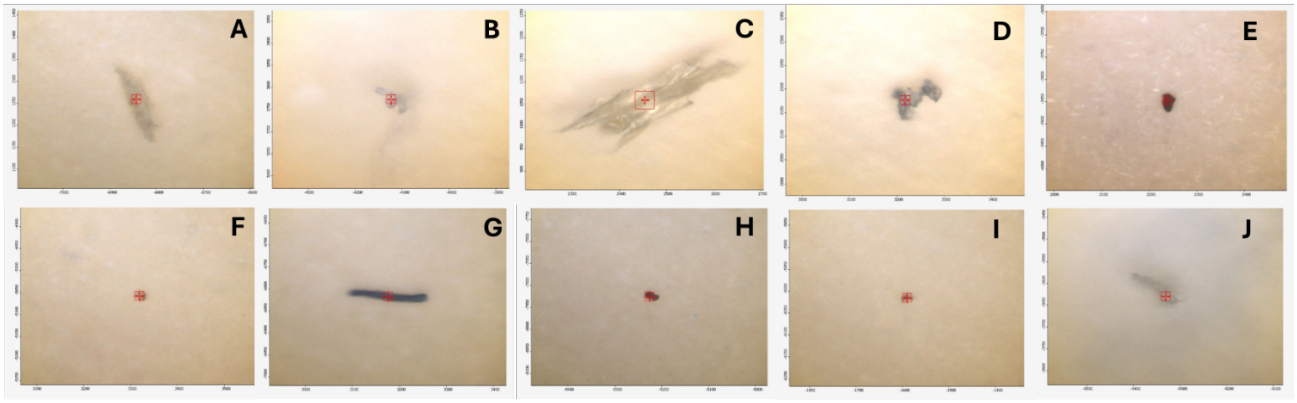

Figure S22. ATR-FTIR particle selection for sample B3.

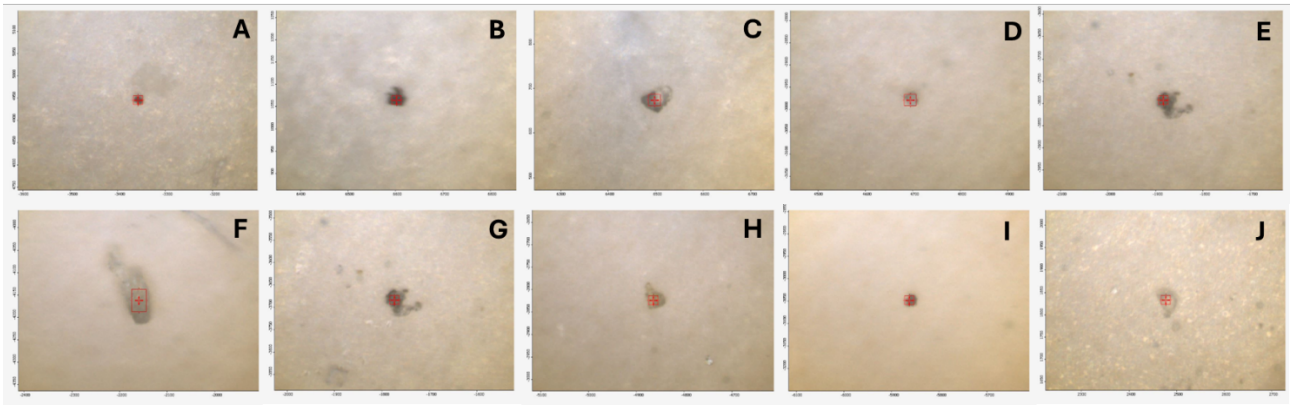

Figure S23. ATR-FTIR particle selection for sample B4. Note that E and G are the same particle, but different images and different spectra readings at different timepoints.

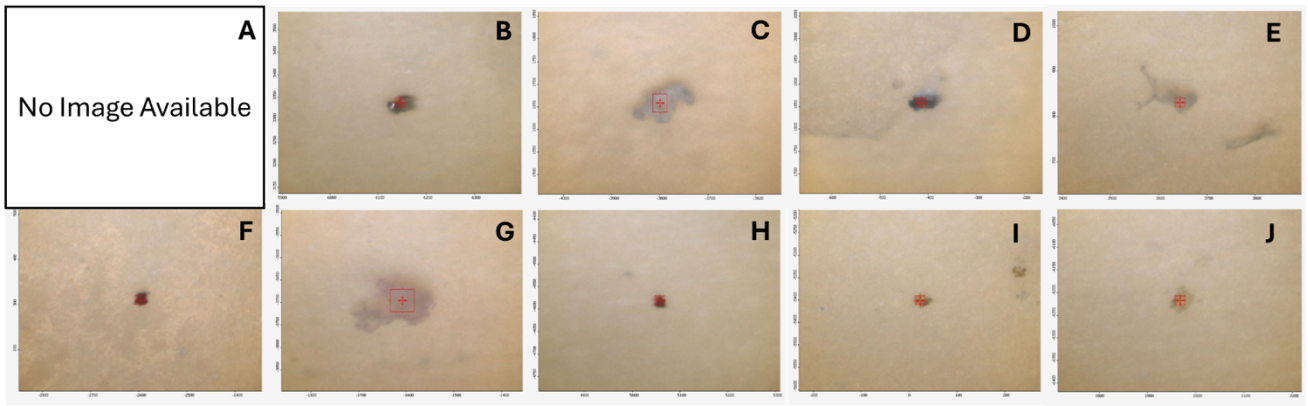

Figure S24. ATR-FTIR particle selection for sample B5.

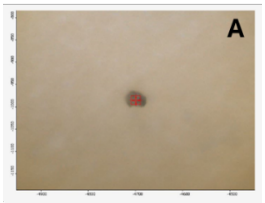

Figure S25. ATR-FTIR particle selection for control sample.

Citations:

1 Prata, J. C. *et al.* A new approach for routine quantification of microplastics using Nile Red and automated software (MP-VAT). *Sci Total Environ* **690**, 1277-1283, doi:10.1016/j.scitotenv.2019.07.060 (2019).

2 R Core Team (2024). _R: A Language and Environment for Statistical Computing_. R Foundation for Statistical Computing, Vienna, Austria. <https://www.R-project.org/>.

3 Huber, P. J. (1964). Robust Estimation of a Location Parameter. *The Annals of Mathematical Statistics, 35*(1), 73-101. https://doi.org/10.1214/aoms/1177703732.